Title

Multi-Scale Investigations of Liquid Flow in a Fractured Basalt Vadose Zone

Authors

Faybishenko, B
Witherspoon, P A
Doughty, C
et al.

Publication Date

1999-03-01

LBNL-42910

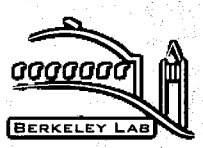

ERNEST ORLANDO LAWRENCE
BERKELEY NATIONAL LABORATORY

Multi-Scale Investigations of Liquid Flow in a Fractured Basalt Vadose Zone

B. Faybishenko, P.A. Witherspoon,
C. Doughty, J.T. Geller, T.R. Wood,
and R.K. Podgorney

Earth Sciences Division

March 1999

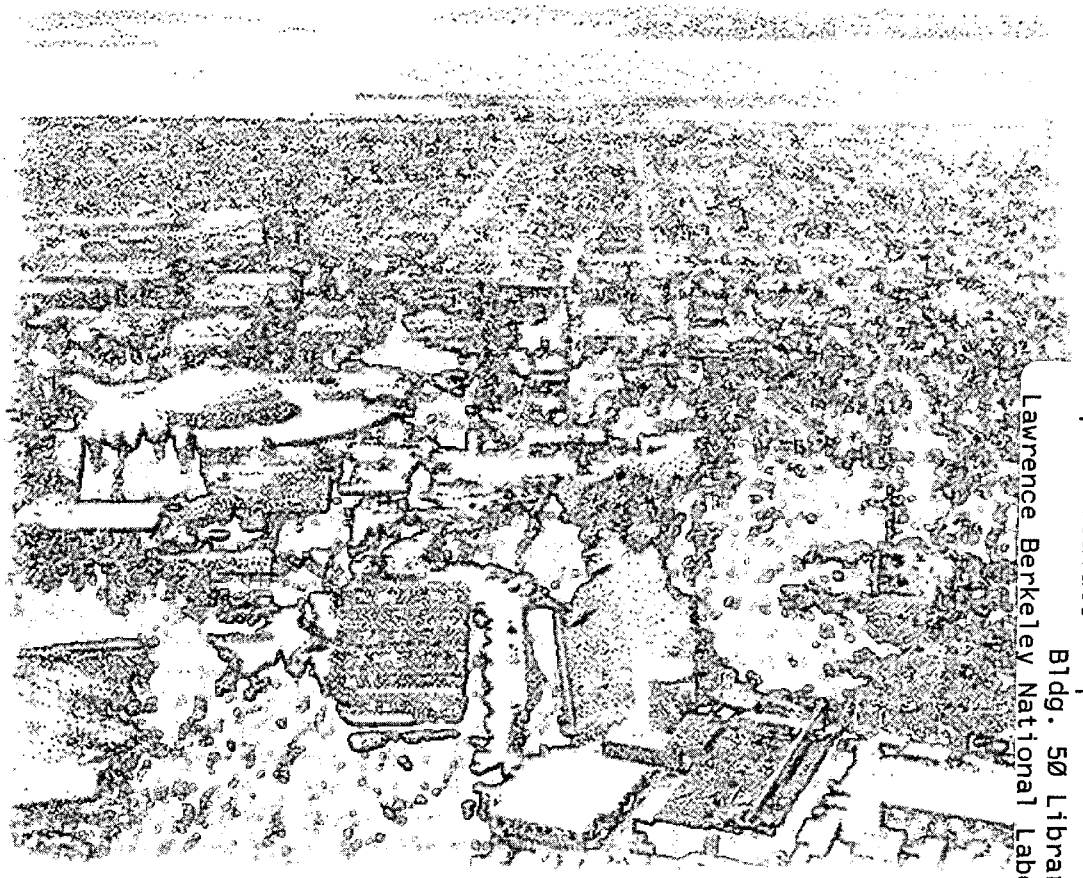

DISCLAIMER

LBNL-42910

Multi-Scale Investigations of Liquid Flow in a Fractured Basalt Vadose Zone

Boris Faybishenko, P. A. Witherspoon, Christine Doughty and Jil T. Geller
Lawrence Berkeley National Laboratory
Berkeley, California 94720

T. R. Wood and R. K. Podgorney
Parsons Infrastructure and Technologies, Inc.
Idaho Falls, Idaho

March 1999

Submitted to AGU Geophysical Monograph "Flow and Transport in Fractured Rocks"

Earth Sciences Division
Ernest Orlando Lawrence Berkeley National Laboratory
University of California
Berkeley, California 94720

The preparation of this report was supported by the Department of Energy, Office of Environmental Management, Office of Science and Technology, Characterization, Monitoring, and Sensor Technology Crosscutting Program, and the Environmental Management Science Program of the U.S. Department of Energy under Contract No. DE-AC03-76SF00098.

Abstract

This paper introduces an approach to the problem of characterizing flow and transport in a fractured basalt vadose zone. We propose the development of physically based conceptual models on a hierarchy of scales. This approach is derived from field investigations that were conducted in the vadose zone of the Snake River Plain in southeastern Idaho. Three scales of ponded infiltration tests were carried out: a Large Scale Infiltration Test (LSIT) conducted at the Idaho National Engineering and Environmental Laboratory (INEEL) (pond area ~26,000 m^2), intermediate-scale infiltration tests (pond area 56 m^2) conducted at the Box Canyon site (near Arco, Idaho), and small-scale infiltration tests (pond area 0.5 m^2) conducted at the Hell's Half Acre Lava Flow Site (near Shelly, Idaho). Laboratory water-dripping experiments were also conducted using fracture models with constant and variable apertures.

We find that, at each scale of investigation, different models for flow phenomena must be used to explain the observed behavior. These models can be used to describe the flow processes on different scales, with no apparent scaling principles evident. To characterize flow phenomena in fractured basalt, we recommend that investigations be carried out on the following hierarchy of scales: elemental, small-scale, intermediate-scale, and large-scale. An elemental component is a single fracture or a block of homogeneous porous medium. Small-scale components include one or a few fractures and the surrounding matrix. Intermediate-scale components include a fracture network and other parts (fracture zones, vesicular lenses, soil, massive basalt, rubble zone) of a single basalt flow. Large-scale components include multiple basalt flows and their surrounding network of rubble zones and sedimentary interbeds.

1. Introduction

Motivation and Practical Importance. For a number of years, several theoretical, experimental, and modeling approaches have been used to investigate flow and transport phenomena in fractured rocks, primarily under saturated conditions (National Research Council, 1996). The modeling methods include continuum approaches that perform volume averaging using the effective continuum (Long et al., 1982; Peters and Klavetter, 1988; Pruess et al., 1985), double porosity (Barenblatt et al., 1960; Warren and Root, 1963), dual permeability, and multiple interacting continua (Pruess and Narasimhan, 1985) concepts, as well as fracture network models (Bear et al., 1993; Dershowitz et al., 1992; Kwicklis and Healey, 1993; Rasmussen, 1987; Smith and Schwartz, 1993). Models developed for saturated conditions cannot, however, describe the significant spatial and temporally varying nature of preferential flow caused by strongly heterogeneous unsaturated flow conditions (Wang and Narasimhan, 1993). A numerical modeling study by Pruess (1998) has shown that flow in an unsaturated fracture with randomly distributed hydraulic parameters does not occur as sheet flow, but rather as a dendritic structure with zones of preferential flow. When Birkholzer and Tsang (1997) did numerical modeling of flow and solute transport in unsaturated media with randomly distributed hydraulic parameters, they determined that even under conditions of steady-state water flow, solute transport exhibits a channeling effect.

Significant efforts have been devoted to the development of alternative models for water flow and chemical transport in heterogeneous media using simple approximations like the transfer function approach (Chesnut, 1994; Jury and Roth, 1990) and percolation theory (Sahimi, 1993). Basic laws governing flow and transport in fractured rock were initially developed from theoretical studies (Snow, 1964; Witherspoon et al., 1980). Yet for most fractured rocks, and particularly the complex system of fractured basalt, it is not possible to develop models directly from first principles; the results of field and laboratory investigations are of primary importance, because they provide the foundations for the basic theories and models governing flow and transport.

To develop an understanding of the flow processes in heterogeneous fractured rocks from experiments, one must recognize the inherent features and limitations of the different types of measurements that can be obtained under field conditions. To monitor flow and transport in the vadose zone, we may use point-type probes, such as tensiometers, thermistors, and suction lysimeters; and geophysical imaging methods, such as seismic surveys, ground penetrating radar (GPR) and 3-D electrical resistivity tomography (ERT) (Hubbard et al., 1997; Majer et al., 1997; Peterson and Williams, 1997). The point-type probes may or may not intersect single fractures. Responses from multiple probes must be combined using either deterministic or stochastic models to develop a macro-scale conceptual model of the flow system (Yeh et al., 1985). The shortcoming of point-type

probe measurements is the difficulty of combining their responses in a meaningful way, such as integrating or volume averaging responses from a number of point measurements, especially when the practicalities of an investigation do not allow for a sufficient number of measurement locations. Geophysical imaging methods complement point-type measurements by providing a spatially distributed view of subsurface conditions. The shortcoming of geophysical methods is their lack of resolution and the difficulty of correlating electromagnetic responses, seismic velocities, etc. to hydrogeologic parameters governing fluid flow. Neither method can be used to observe flow in single fractures or fluid movement at the fracture-matrix interface in sufficient detail to accurately represent transport. Field measurements generally provide only average characteristics of the rock and fracture properties over space and time. The actual resolution of the measurements and the volume of rock involved in averaging remain unknown. It is also important to keep in mind that, in contrast to porous media, different geological, mechanical, and geochemical processes govern the physics of flow in fractured rocks, such as basalt. The wide variety of processes controlling flow in fractured basalt at different scales makes conventional scaling procedures not applicable.

Basaltic rocks are widely distributed in the United States and throughout the world (Korvin, 1992; Long and Wood, 1986; Tomkeieff, 1940). Our investigations were conducted in fractured basalt of the Eastern Snake River Plain of southeastern Idaho near the Idaho National Engineering and Environmental Laboratory. Contaminants of concern, such as VOCs (TCE, carbon tetrachloride, etc.) and radionuclides (Cs, Sr, U, Pu, etc.), were buried in soils overlying the basalt vadose zone or were injected directly into basalt using wells and pits. The prevailing thought at the time of burial was that contaminants would not migrate downward to the underlying Snake River Plain aquifer. However, contaminants have been found in perched water zones, interbed sediments, and the aquifer. Currently, several INEEL sites are being remediated and instrumented for long-term monitoring. It has become apparent that monitoring technologies, characterization methods, and prediction procedures developed for porous media are not sufficient to treat fractured basalt.

Objectives. The objectives of this paper are to introduce a new approach to the multi-scale characterization of flow and transport in the fractured basalt of the vadose zone and to develop physically based conceptual models on a hierarchy of scales. We will illustrate this new approach using results of field and laboratory investigations conducted in the fractured basalt near the INEEL. The results were obtained from field tests carried out at three different sites: (1) small-scale infiltration tests (ponded area 0.5 m^2) conducted at the Hell's Half Acre site (near Shelly, Idaho), (2) intermediate scale infiltration tests (ponded area 56 m^2) conducted at the Box Canyon site (near Arco, Idaho), and (3) a Large Scale Infiltration Test conducted near the INEEL Radioactive Waste Management Complex (ponded area ~26,000 m^2). In addition to these field tests, laboratory investigations included measurements on fractured basalt cores and small-scale dripping experiments in fracture models.

The paper briefly describes the geology of the Snake River Plain basalt flows and the various processes involved in flow and transport in fractured basalts. We introduce the hierarchy of hydrogeological scales for use in constructing models and developing observational methods. A description of the results from laboratory water dripping experiments on the elemental scale is followed by an interpretation of the results from the three field infiltration tests. We conclude with a summary and present some practical applications.

2. Geology of the Snake River Basalt

2.1. General Information

The Snake River Plain is primarily composed of fractured Quaternary basalts, interlayered with sedimentary deposits (Knutson et al., 1993; Lindholm and Vaccaro, 1988). Multiple basalt flows (Figure 1) within a flow unit were formed by closely related eruption events (Lindholm and Vaccaro, 1988). Individual basalt flows are typically highly fractured, with a thickness that ranges from less than 1 m to more than 30 m, and an areal extent of up to several thousand square meters. Fracturing was caused by thermal contraction as the flow cooled and formed polygonal, often hexagonal, columns (Korvin, 1992). The upper portion of the flow is usually densely fractured, even rubblelized (Grossenbacher and Faybishenko, 1995; Lore, 1997), as a result of exposure to the atmosphere, which produced an increased cooling rate. Therefore, fracture density decreases toward the center of the flow. The lower half of the flow contains fewer fractures because of a slower cooling rate. When the basalt columns were exposed to weathering over geologic time, their surfaces weathered to breccia and were often covered with sediments that separated the flow units (Welhan and Reed, 1997). Sedimentary interbeds may have a significant lateral extent (often exceeding that of the individual basalt flows) and their thickness ranges from a few centimeters to as much as 15 m. Geophysical logging suggests that the total thickness of the basalt in the Snake River Plain may exceed three kilometers. In the region near INEEL, the depth to the water table of the regional aquifer ranges from 60 to 200 m.

The unusually complicated geometry of basalt flows with wide contrasts in the permeability of dense basalt and highly fractured rubble zones has raised concerns over how such systems should be characterized. For the Columbia basalt flows in the State of Washington, the Department of Energy (1986) has identified four domains for basalt flows: (A) the domain of a single fracture; (B) the domain of multiple fractures within the entablature and colonnade; (C) the domain of entablatures, colonnades, and flow tops; and (D) the domain of multiple basalt flows. Note that Domains A, B, and C are restricted to a single flow. We have found this classification useful for examining the

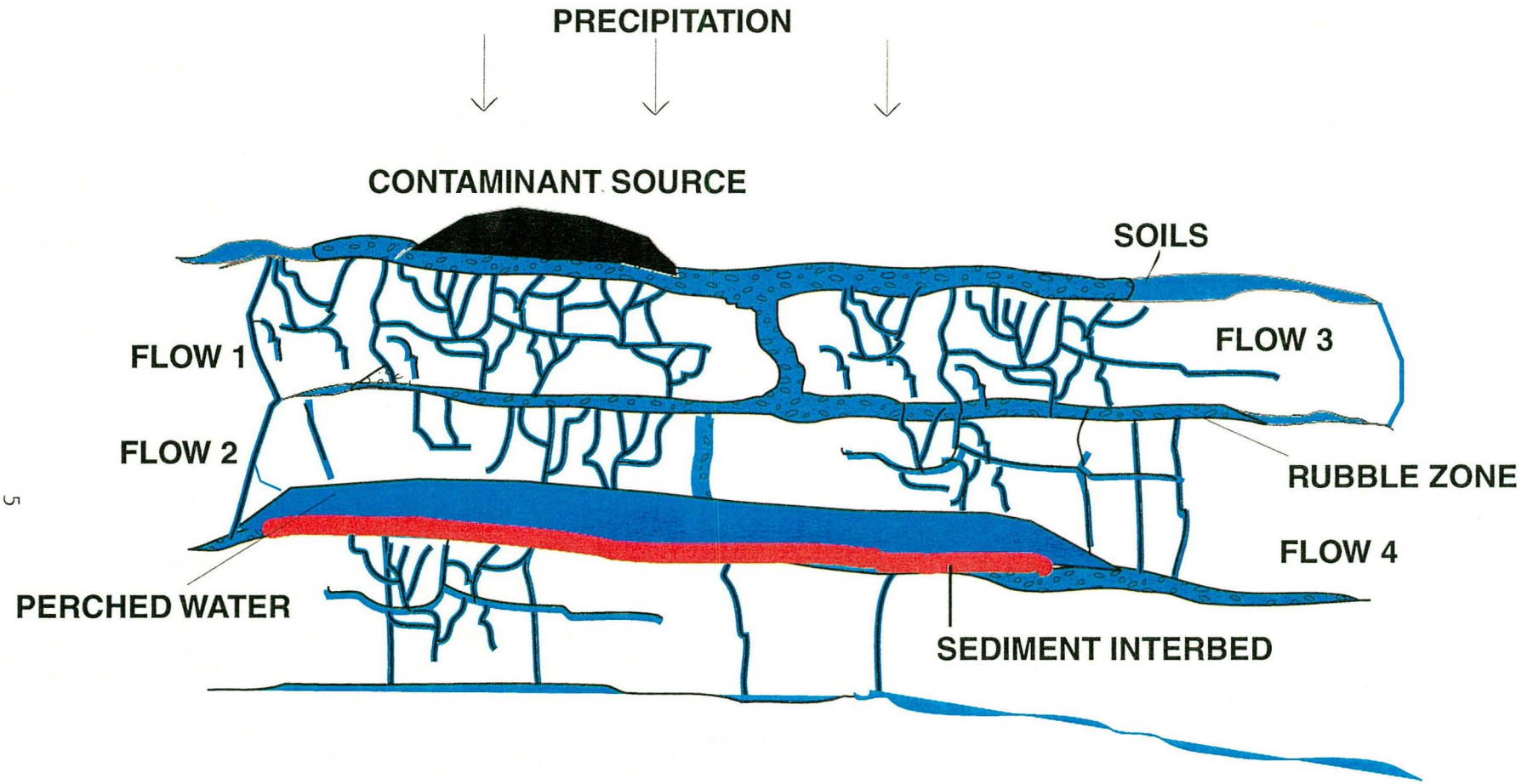

Figure 1. Schematic illustration of water flow and contaminant transport in fractured basalt, including flow through inter-basalt rubble zones and through intra-basalt fractures. Note that perched water zones are formed above the sedimentary layer.

basalts of the Eastern Snake River Plain, and we have used it in developing the concept of a hierarchy of hydrogeological scales.

2.2. The Research Sites

Hell's Half Acre Site. The site is located within the Hell's Half Acre (HHA) Lava Field in southeastern Idaho. The site consists of an overhanging basalt block on the edge of a collapsed lava tube. The basalt is moderately vesicular to dense, with a single fracture exposed on the surface of the block. The fracture bifurcates in the lower part of the block, resulting in two fracture traces on the underside. A horizontal fracture, which intersects the vertical fracture, is exposed on the face of the block, approximately 25 cm from the underside. The physical layout of the site permitted access to the top, front, and underside faces of the basalt block, thus allowing for detailed instrumentation and data collection of both infiltration and outflow rates from the fracture. The access to the underside also allowed for collection of time intervals between drips falling from discrete locations along the fracture, which were then used for an analysis of observed chaotic data.

Box Canyon Site. The Box Canyon site is located in the Eastern Snake River Plain near the INEEL (Long et al., 1995). Minimal soil cover and a nearby cliff-face exposure provide an excellent opportunity to study the relationships between the fracture geology and the hydrogeologic response to the infiltration tests. The surface of the Box Canyon site consists of exposed weathered basalt and soils (clays and silts), which infill the near-surface fractures and basalt column joints (Engelder, 1987). The depth to the regional aquifer is about 200 m at the Box Canyon site, with a perched water zone located at a depth of about 20 m. Along the cliff face, about 30m from the infiltration pond, two distinct basalt flows with a rubble zone between them are exposed. The fractured basalt vadose zone is comprised of the following geological components: a surface sedimentary layer including basalt rubble, upper vesicular zones with numerous near-surface soil-infilled fractures, massive basalt, vertical and sub-vertical column-bounding joints, horizontal and subhorizontal fractures, central fracture zone, lower vesicular zone, and underlying rubble zone [Faybishenko et al., 1998].

Large Scale Infiltration Test Site. The LSIT site is located 1.4 kilometers south of the Radioactive Waste Management Complex (RWMC) at the INEEL. The RWMC includes one of the largest subsurface waste disposal facilities in the DOE complex. Past disposal of low-level, mixed, and transuranic radioactive wastes occurred by direct discharge or burial in shallow, unlined pits and trenches within the surficial sediments. Flooding of the RWMC has occurred three times in the past, potentially increasing the downward mobility of the subsurface contaminants. The time required for contaminant migration to reach the aquifer is fundamentally significant to management decisions regarding remediation options.

In 1994, the INEEL conducted the LSIT to investigate hydrologic properties of the vadose zone basalts. The vadose zone thickness near the RWMC is about 190 m. The LSIT site consists of a bermed basin 183 m in diameter, which contained 32 million liters of water during the test. Beneath the basin is a thick sequence of stacked basaltic lava flows with the first major interbed at depth of 55 m. A total of 70 wells were drilled for the test primarily along four axes extending radially from the basin, with most terminating in the sedimentary interbed. Therefore, the LSIT test investigated the hydrologic properties of a hypothetical "cylinder" of basalt that is 55 m thick and 183 m in diameter.

3. Hierarchy of Hydrogeological Processes

3.1. Flow Processes and Monitoring Techniques for Different Scales

In our investigations, we have found that on different scales a variety of conditions affect flow processes in fractured basalt. Regional groundwater flow through the aquifer is commonly studied on a very large scale, where observation wells are thousands of meters apart and model domains encompass hundreds of square kilometers. At this scale, the aquifer is highly transmissive and anisotropic, with nearly all the permeability arising from the network of rubble zones surrounding individual basalt flows. Bruno et al. (1992) found that fractal models can describe the shape of basalt flows. Pumping tests have revealed that the horizontal permeability is higher than the vertical because of the large aspect ratio of individual basalt flows (Welhan and Reed, 1997). Because of anisotropy, large-scale infiltration may lead to lateral spreading of infiltrating water. The sedimentary interbeds are of relatively low permeability and may act as aquitards for perched water zones, in which contaminants can accumulate.

In contrast, at the intermediate scale, we may be interested in a site that has neither a network of rubble zones to provide high permeability flow paths nor a sedimentary interbed to block flow. At this scale, we investigate the intra-basalt flow fracture pattern. Figure 2 shows a photograph of the basalt outcrop at the Box Canyon site and the corresponding lithological crosssection, which identify the main geological features of the vertical section. These features include a flow-top breccia, vesicular and massive basalt layers, a central fractured zone, a rubble zone, and vertical and horizontal fractures (Faybishenko et al., 1998). During infiltration from rainfall and snowmelt, sediment particles have migrated into the subsurface and accumulated in both vertical and horizontal fractures to a depth of at least 2-3 m. As water moves through these soil-filled fractures, it can be imbibed into the adjacent porous, vesicular and dense basalt matrix. Water may also flow laterally in the vesicular layers and the central fractured zone. Below the central fractured zone, the downward flow is more restricted on account of the

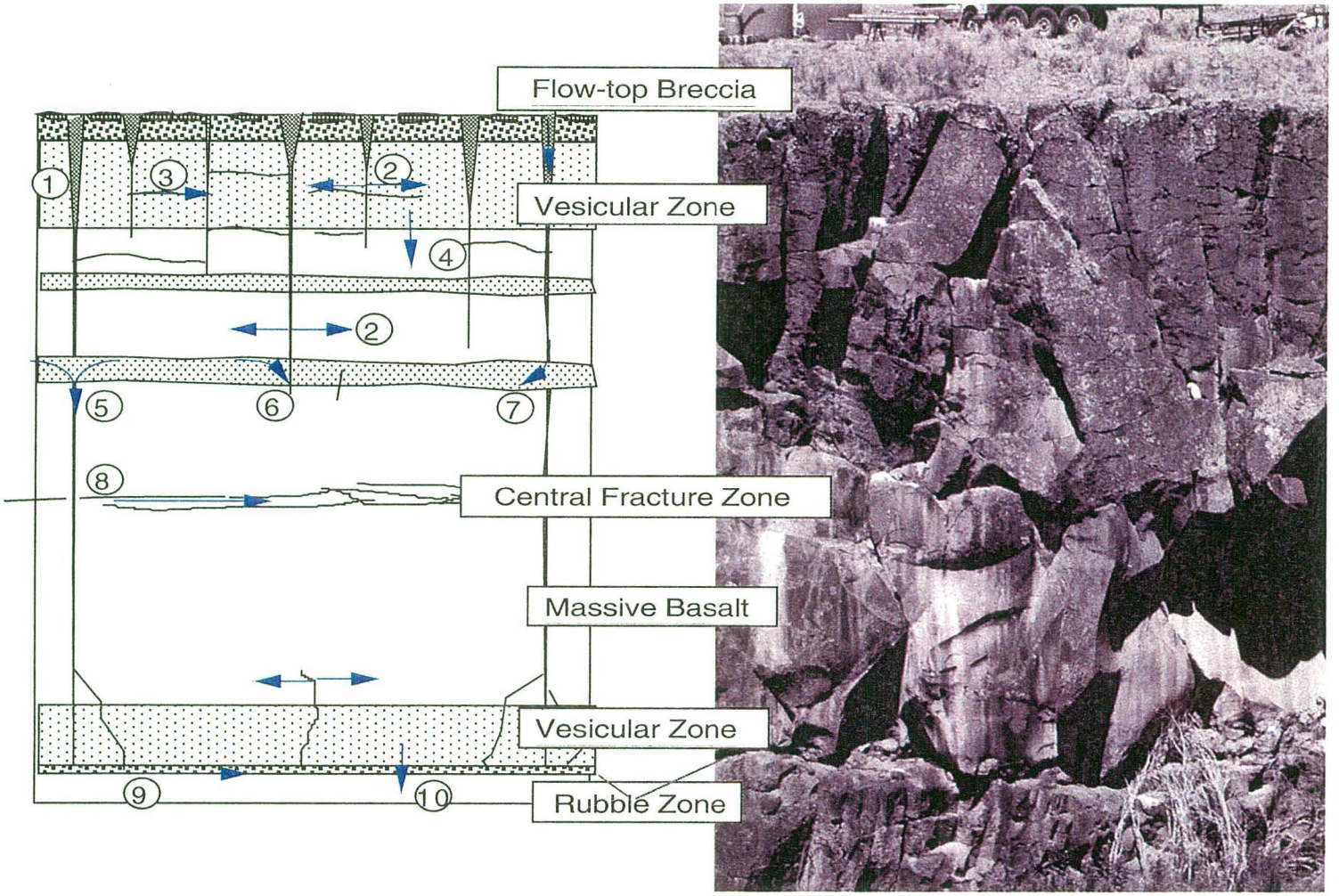

Figure 2. Geological features and processes of water flow and chemical transport in fractured basalt: 1-flow through near-surface soil-infilled fractures, 2-fracture-to-matrix diffusion, 3-flow in a horizontal fracture connecting vertical fractures, 4-vesicular basalt-to-massive basalt diffusion, 5-funneling effect, 6-vesicular basalt-to-nonconductive fracture diffusion, 7-conductive fracture-to-vesicular basalt flow and diffusion, 8-lateral flow and advective transport in the central fracture zone, 9-lateral flow and advective transport in the rubble zone, and 10-flow in the underlying basalt flow.

wide spacing of the fractures in the lower part of the basalt flow. Figure 2 shows the presence of dead-end, nonconductive fractures, which are difficult, if not impossible, to identify from point-type measurements in boreholes. Contaminants can be trapped in these dead-end fractures and then diffused into the basalt matrix.

Because fractured basalt is characterized by drastic differences in permeability of fractures and matrix, the results of hydraulic tests depend on the scale that is affected by these field or laboratory experiments. For example, if we take a core containing a fracture, the permeability may be very high, but the permeability of this fracture when determined under field conditions may appear to be much less, because the fracture may not be connected to the main water pathway. In addition to the effects of the flow geometry and lithology, the flow processes in the vadose zone are also controlled by variations in moisture content and permeability of both the fractures and matrix (Mantoglou and Gelhar, 1987a,b). Because the relationship between moisture content and permeability of partially saturated rocks is nonlinear (Pruess and Tsang, 1990; Persoff and Pruess, 1995), the flow processes in the vadose zone are also nonlinear. It is known from the theory of nonlinear dynamics that a combination of several nonlinear processes may lead to chaotic variations of the system parameters (Abarbanel, 1996; Tsonis, 1992). In such systems, small changes in initial and boundary conditions may create new macro-flow structures for different flow processes with no apparent scaling principles involved (Gleick, 1987; Haken, 1983).

Because a variety of flow and transport processes occur in different parts of the fractured basalt and rubble zones, the overall system is complex, requiring sophisticated models to describe it. In order to obtain realistic data to develop and calibrate such models, it is necessary to use the proper instrumentation consistent with the nature of the hydrogeological processes that control the behavior of the total system. However, we face the problem of inconsistency between the scale of measurements and the scale of flow and transport processes in fractured basalt. For example, the radius of influence for single probes (e.g., tensiometers, suction lysimeters) used to monitor flow and contaminant transport in the vadose zone is about to 30-40 cm. Obviously, this is much smaller than the rock volume being characterized. Thus, single probes used to investigate strongly heterogeneous and fractured rocks only interrogate a limited volume, and the collected data may not be representative of the total system.

As the investigated rock volume increases, additional point measurements over larger volumes may not improve the characterization of the medium. This is because the number of monitoring points is limited in a practical sense, and these points may be located in different parts of the system, which are not hydraulically connected. In order to determine how well the point measurements represent the system, we need other independent information. A promising method for obtaining this information is to combine point-type measurements with geophysical methods, such as GPR and ERT. A GPR method can be used to determine the spatial distribution of wetted zones in basalt

between boreholes that are separated from 2 to 4 m, but cannot be used in monitoring the dynamics of fast fluid flow in individual fractures (as will be shown below in Section 7).

The hydraulic properties of saturated geologic media are known to correlate with the scale of observations from the laboratory scale to thousands of meters (Dagan, 1989; Gelhar, 1993; Neuman, 1990; 1994; Molz and Boman, 1995). However, the approach used for scaling of saturated hydraulic parameters may not be applicable for the unsaturated fractured basalt, because: (1) different hydraulic processes govern flow on different scales, and (2) the scale of measurements in the vadose zone (using point-type, near-borehole, and cross-borehole measurements) is inconsistent with the scale of flow processes in the field. Heffer and Koutsabeloulis (1993) determined that despite the presence of a scaling relationship for the fracture frequency and the fracture trace lengths from single cores to thousands of meters, the scaling of hydraulic properties determined for small scales terminates for the larger scales. Thus, in order to provide a proper description of the processes governing flow and transport in basalt, we will use a hierarchy of scales with appropriate models and methods of investigation

3.2. The Concept of a Hierarchy of Hydrogeological Scales

The concept of a hierarchy of scales for investigation of fractured rocks is based on the assumption that the whole system is composed of a number of components that behave differently on different scales. In describing flow problems in basalt, we propose a four-level hierarchy of hydrogeological components, which includes elemental, small-scale, intermediate-scale, and large-scale components. The relationship between these components is illustrated in Figure 3.

Elemental components of the flow system include a single fracture or a block of porous medium (matrix). Elemental components can be studied using small laboratory cores, fracture replicas, or point-size probes under field conditions. Results of experiments on this scale can be used to describe the details of specific flow and transport processes in fractures, matrix, or fracture-matrix interaction (Ho, 1997). Some examples of these flow processes are: (1) water dripping from a fracture under field conditions in boreholes, tunnels, caves, and other underground openings; (2) film flow (Tokunaga and Wan, 1996) and water meandering along a fracture surface in laboratory experiments (Su et al., 1998); and (3) water dripping within flow channels, or flow intermittence, along a fracture surface in laboratory experiments. The size of the elemental component is from a few centimeters to 10-20 cm.

Small-scale components include a volume of rock within a single basalt flow with one or a few fractures. Results of field experiments on this scale can be used to describe in detail some of the flow and transport processes in a single fracture or a few intersecting fractures. Small-scale infiltration experiments are conducted to take into account

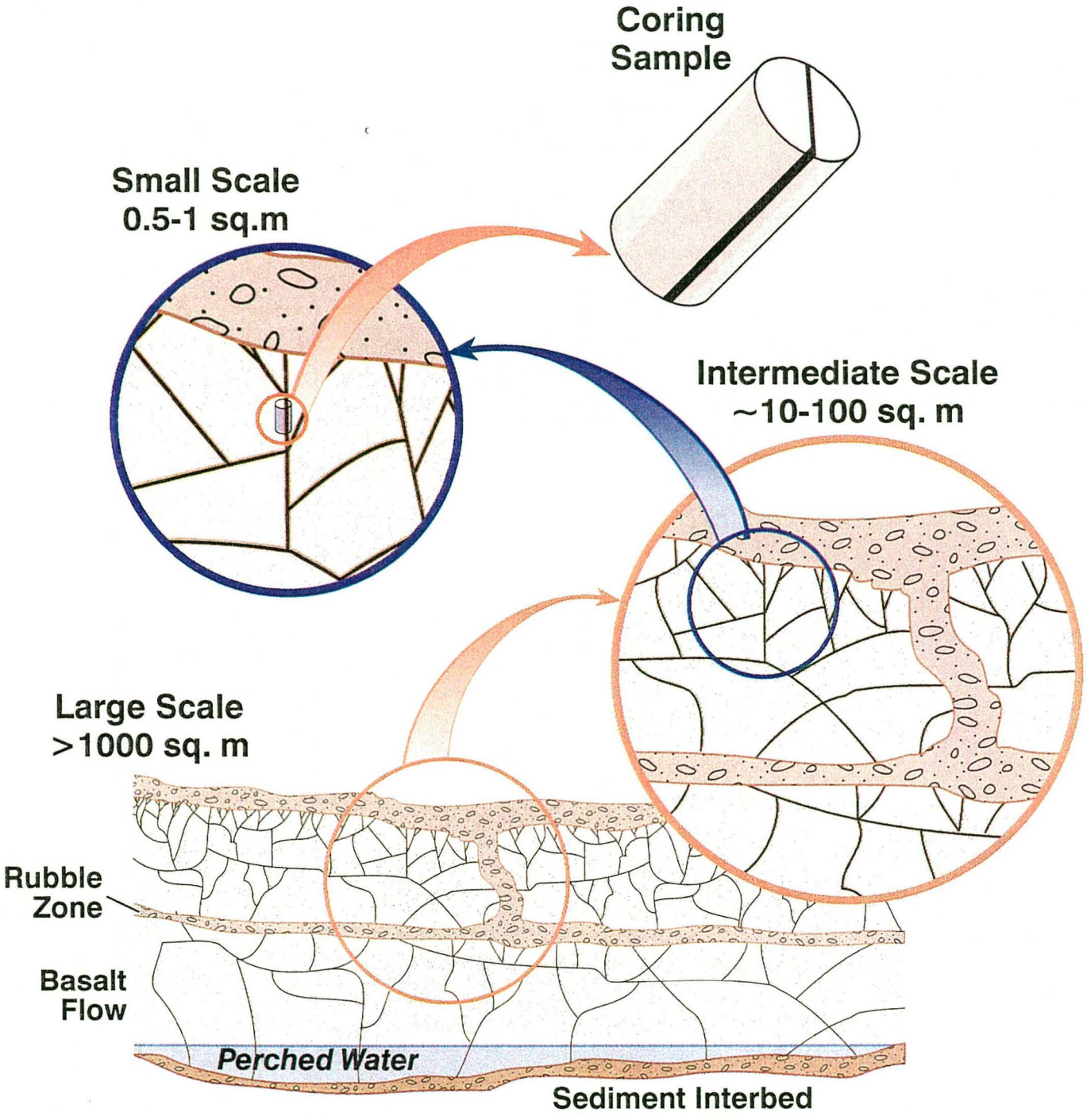

Figure 3. A four-level hierarchy of scales of hydrogeological components in fractured basalt

fracture-matrix interaction, water dripping phenomena, and small-scale averaging of flow rates and water pressures measured in fractures and matrix. The areal extent of small-scale components is approximately 0.5-1 m^2.

Intermediate-scale components include the volume of rock within a basalt flow involving all types of fractures, including the fractured flow top, dense flow interior, the less fractured flow bottom and fractures intersecting the basalt flow and a rubble zone. The results of field experiments at this scale can be used to describe all flow and transport processes within a single basalt flow. The essential issue is the study of flow in the fracture-network within a single basalt flow. We also study other basalt-flow features such as vesicular or massive basalt, fracture zones in the upper and lower fractured colonnade, and the central fractured zone or entablature. The areal extent of intermediate-scale components is approximately 10-100 m^2.

Large-scale components involve the volume of rock containing several basalt flows and the rubble zones between them. At this scale, we can study flow in the fracture networks and regional hydrogeological processes, which are affected by the network of vertical and horizontal rubble zones, as well as sedimentary interbeds. The areal extent of a large-scale component usually exceeds 1,000 m^2.

In order to analyze the time-series data sets obtained from monitoring water-dripping phenomena in laboratory and small-scale field infiltration tests, we used the methods of nonlinear dynamics, described below.

4. Using Nonlinear Dynamics Methods to Analyze Time-Series Data Sets

A conventional method to analyze time-series data is to conduct a Fourier type analysis, which decomposes a signal into different frequency components. This method is effective for linear systems, but the resulting frequency components may appear as noise for deterministic-chaotic functions (Abarbanel, 1996), because there are an infinite number of frequencies comprising chaotic motion. The Fourier transformation is used to analyze time-varying scalar signals with no assumption about the underlying physics of the processes. In contrast, the methods of nonlinear analysis assume that (1) the time-varying function contains information about the processes affecting this function, and (2) multi-dimensional vectors describe the time evolution of the function. The space in which these vectors evolve is called a state space or phase space, for which the dimension is an integer (Abarbanel, 1996).

In unsaturated rocks, useful phase-space variables are moisture content, water pressure, and flow velocity, which depend on each other in a nonlinear fashion. Another variable, which one can measure directly in laboratory and small-scale field experiments, is a water dripping frequency. The nonlinear flow processes in the fractured rock vadose

zone are subject to chaotic fluctuations, implying that trajectories through phase space may not be steady or periodic. Furthermore, because the vadose zone processes are dissipative, the volume of a phase space occupied by the trajectories decreases with time. For such a system, the basic idea behind the nonlinear time-series analysis is to reconstruct the phase-space and then plot an attractor in the phase space. The attractor is a set of points in phase-space toward which nearly all trajectories converge (Grassberger and Procaccia, 1983). In other words, the attractor describes typical system behavior. An attractor for a chaotic system often has a fractal structure, and it is called a strange, or chaotic, attractor (Moon, 1987).

Because the phase-space variables depend on each other, the time-series analysis of any one of those variables may give us an understanding about the physics of the whole system. Therefore, we choose a single scalar variable P (e.g., water pressure, dripping frequency) and plot its trajectory through a pseudo phase space whose dimensions are $P(t)$, $P(t+\tau)$, $P(t+2\tau)$, $\ldots P(t+(n-1)\tau)$. In order to plot the attractor, we need to determine the correlation time, τ, which is the time interval between data points when the relationship between the points almost vanishes, and the embedding dimension, n, of the attractor. The embedding dimension is the dimension of the pseudo phase space needed to unfold the attractor of a nonlinear system from the observation of a scalar signal. That is, it is the number of coordinates required in order that the orbits composing the attractor no longer cross one another in the pseudo phase space. The method of false nearest neighbors (Kennel et al., 1992) is used to determine the embedding dimension of the attractor.

Before describing n and τ in more detail, we will show several simple examples of 2D attractors, which are the relationships between the value of the time-varying function P at the time t and its value at the time $t + \tau$. For example (Faybishenko, 1999), for the sine function, the attractor is an ellipse (Figure 4a). For the sine function with a small random component added, the attractor has some points scattered around the ellipse (Figure 4b). For the random function with a uniform probability density function, the attractor covers the whole phase-space (Figure 4c). For the deterministic chaotic system described by a system of well known Lorenz equations, the attractor has a well defined, but complex, pattern (Figure 4d). This figure illustrates that a scatter of data points on the attractor characterizes the contribution of a random component in the original time-series data set.

For a complex system, an attractor may have three or more dimensions, but we can plot attractors only in a 3D phase space using the coordinates $P(t)$, $P(t + \tau)$, and $P(t + 2\tau)$. Hence, the 3D view of an attractor with $n>3$ can give us just a general idea about the attractor. It turns out that if an attractor depends on many variables (corresponding to a high-dimensional pseudo phase space with $n>>3$), its projection into 3D space will tend to fill up the whole space, making the chaotic system resemble a purely random system.

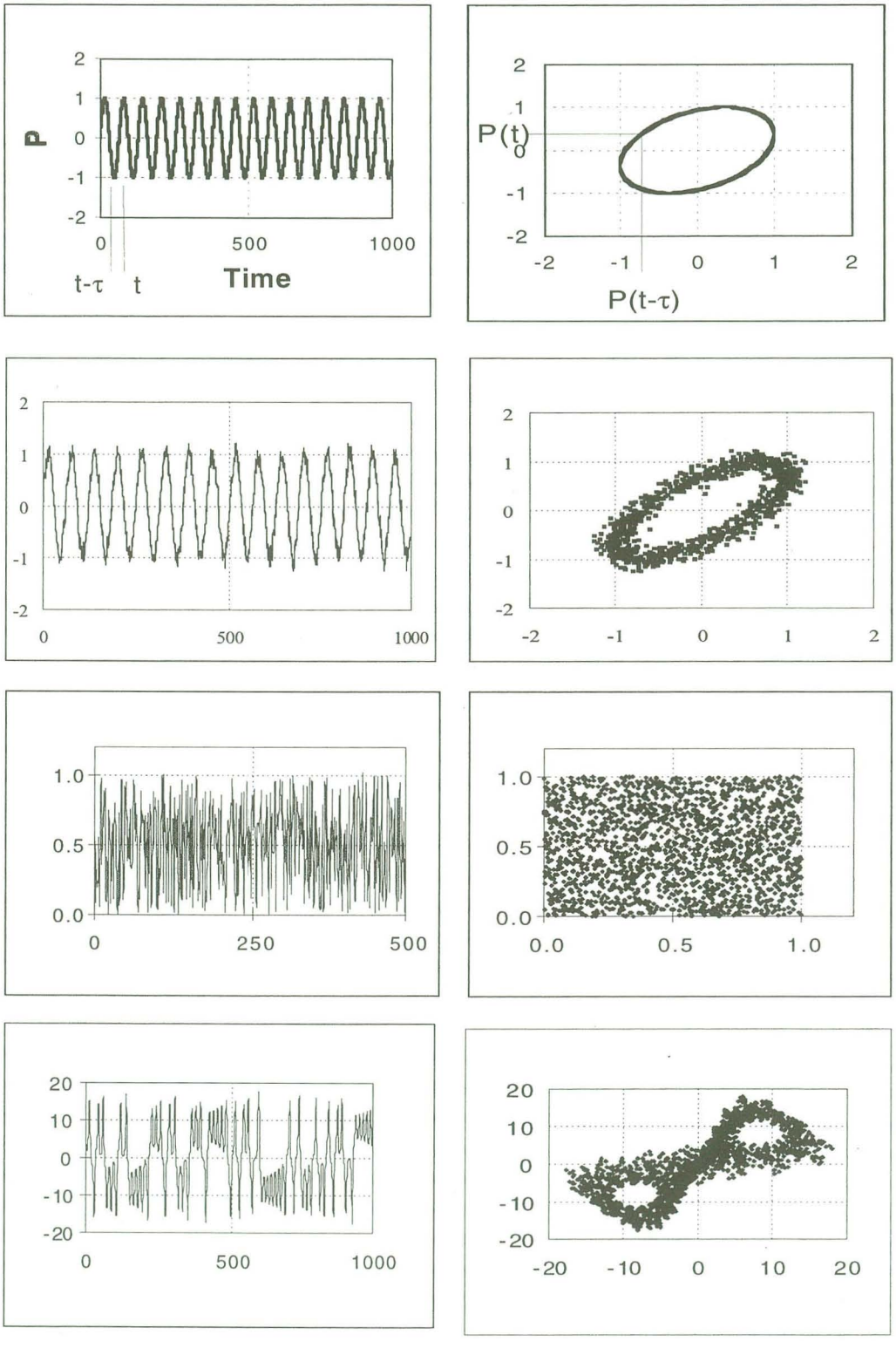

Figure 4. Time-series functions (left) and their two-dimensional attractors (right): (a) sine function, (b) sine function with noise, (c) random function, and (b) chaotic system from a set of Lorenz equations.

The correlation time τ can be determined using the average mutual information function (Kennel et al., 1992). This function describes the information learned about one observation from another observation, when averaged over all measurements. In other words, we determine the amount of information, in bits, learned about the point $P(t+n\,\tau)$ from the measurements of $P(t+(n-1)\tau)$. The first minimum of the average mutual information function versus τ is used to determine an optimum correlation time.

Despite the fact that we cannot precisely identify all factors and processes affecting the system, we can determine the system bounds within which the system is supposed to behave over long periods of time. Some diagnostic parameters (capacity dimension, correlation dimension, Hurst exponent, and Lyapunov exponent) are used to recognize whether the system contains a deterministic-chaotic component in otherwise random-looking time-series data (Moon, 1987).

Chaotic phenomena are common in the fields of physics, ecology, biology, economics, geology, etc. (Tsonis, 1992). However, the claims for chaos in hydrologic systems have to be carefully assessed, because the number of observations are often limited and not sufficient to calculate diagnostic parameters of chaos (Pasternak, 1996). Identifying the chaotic nature of a system enables the determination of the number of variables that must be measured to define behavior. It also indicates that for chaotic systems, which are sensitive to initial conditions, only short-term predictions of the time-trend of the data functions are possible. The long-term predictions of the time-series of the data functions are not possible, but the attractors can be used to determine the bounds of the parameters characterizing the long-term behavior of the system.

5. Laboratory Investigations of Flow in Fracture Models

5.1. Test Design

Water seepage within a fracture can proceed through channels that undergo cycles of snapping and reformation under low-flow conditions even in the presence of constant boundary conditions (Su et al., 1998). Figure 5 shows a cycle of water dripping within a flow channel along a dense basalt fracture surface mated to a transparent replica of the other fracture half (Geller et al., 1996). In order to investigate the physics of this time-varying intermittent flow under laboratory conditions, we designed a series of water dripping tests within smooth-walled and rough-walled transparent fracture models having sub-millimeter apertures (Figure 6). Water was supplied at constant rate through a capillary tube inserted into the fracture models. The time variation of the water pressure at the tube entrance was measured over a range of flow rates. Video images of flow

Figure 5. Video images of a cycle of water dripping within a flow channel along a dense basalt fracture surface mated to a transparent replica of the second half of the fracture. Time is given in the left-bottom corner of each image. Water was applied at 0.33 mL/hr to the top of the fracture. Fluorescein was added to the water to promote visualization by near-UV light. The fracture was inclined at 20° from the horizontal.

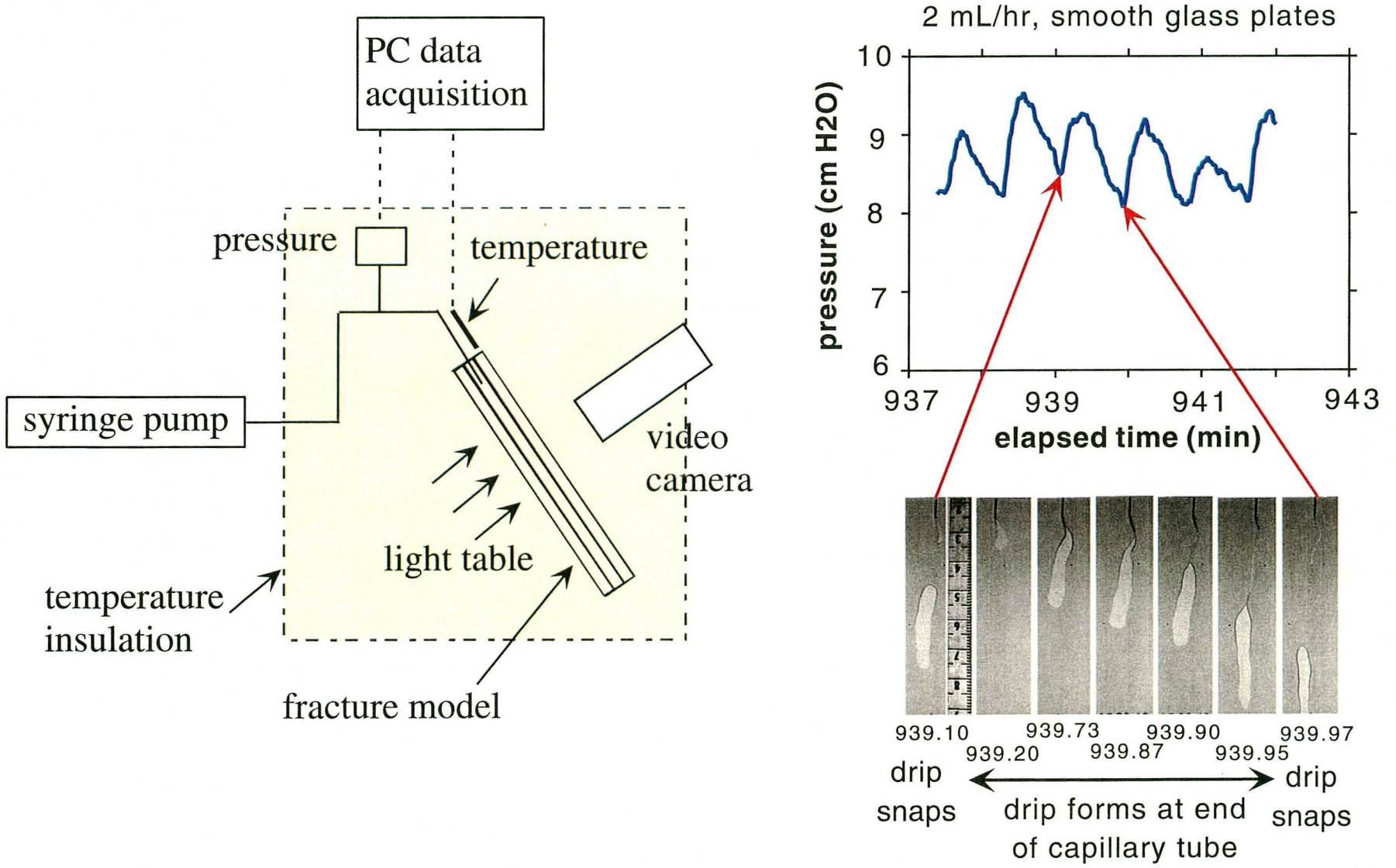

Figure 6. Experimental setup for monitoring water-dripping in fracture models: (a) The fracture model is 20 cm x 30 cm glass plate pairs, smooth or textured, separated by 0.35 mm shims; the model is inclined 60° from the horizontal; (b) Time-series of water pressure measured at the entrance to the capillary tube and corresponding video images of drip formation. Note that the water thread snaps when the pressure is minimal. We assume that the weight of the water drop overcomes capillary forces arising from the presence of the small fracture model aperture.

confirmed that the pressure fluctuations occurred in response to flow behavior, as drops formed and detached within the flow channel (Figure 7). Pressure data were also acquired for dripping from the tube open to atmosphere.

5.2. Test Results and Conceptual Model of Flow in Fracture Models

Figure 7 compares the time variation of pressure and corresponding attractors for the flow rate of 0.25 ml/hr for three different cases of water flow through a 0.18 mm ID capillary tube: (1) open air, (2) a constant aperture fracture model (0.35 mm separation between smooth glass plates), and (3) a variable aperture fracture model (textured-glass plates). Comparison of the attractors in Figure 7 shows a progression of the systems from noisy to more deterministic-chaotic, as the geometry surrounding the dripping water becomes more complex. Calculation of the diagnostic parameters of chaos confirms that the magnitude of the random component decreases and the contribution of the deterministic component increases from the open air to constant aperture to variable aperture system. Pressure data at higher flow rates (up to 10 mL/hr) and for larger diameter tubes (0.8 mm I.D.) had an increased random component.

These experiments show that under certain conditions, flow behavior along water channels in a fracture model has a significant chaotic component. For such systems, a deterministic-chaotic model with a random component should describe flow behavior.

6. Small-Scale Infiltration Test

6.1. Test Design

The objective of the field investigation conducted at the Hell's Half Acre site was to evaluate flow processes on the meter scale (Podgorney et al., 1997; 1999). The research site consists of an overhanging basalt block (thickness approximately 1 meter and an areal extent of 2 by 3 meters) on the edge of a collapsed lava tube. A single vertical fracture is exposed at the surface of the basalt block. This fracture bifurcates in the lower part of the block, resulting in two fracture traces on the underside. A horizontal fracture, which intersects the vertical fracture, is exposed on the face of the block, approximately 25 cm from the underside.

A 40 x 80 cm infiltration pond was built on the upper surface of the basalt block, surrounding the surface expression of the fracture (Figure 8). The site was instrumented to collect extensive data sets to describe both the temporal and spatial variations of the

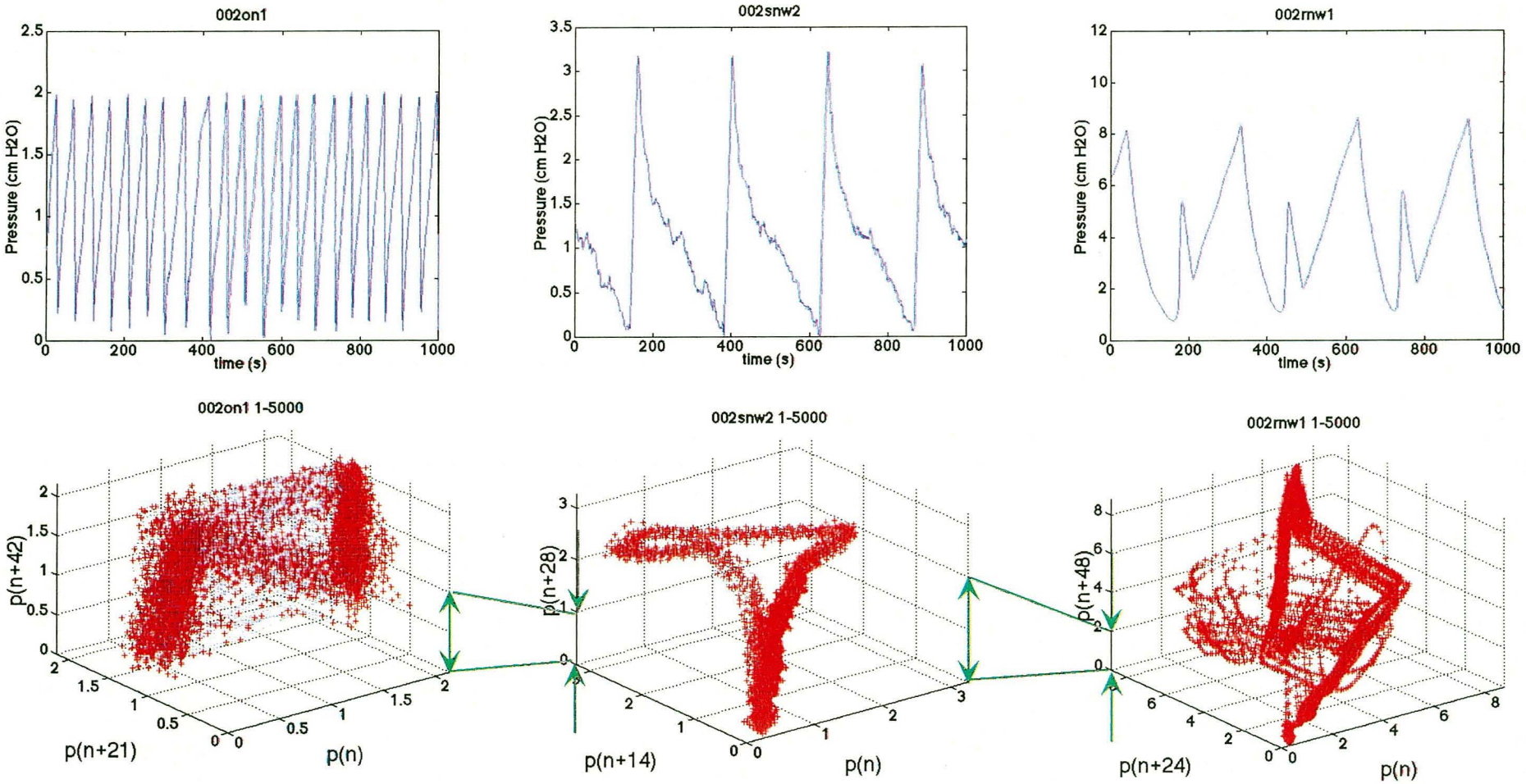

(a) Open Air

(b) Constant Aperture (0.36 mm)

(c) Variable Aperture (0-1 mm)

Figure 7. Time-series data (above) and attractors (below) for 0.25 mL/hr flow rate through 0.18 mm ID capillary tube: (a) Open-air drips, (b) Constant aperture, 0.35 mm, glass plate pair, and (c) Variable aperture, 0-1 mm, fracture model. As the geometry surrounding the tube becomes more complex, the magnitude of pressure fluctuations increases and the attractors change from noisy to more deterministic chaotic.

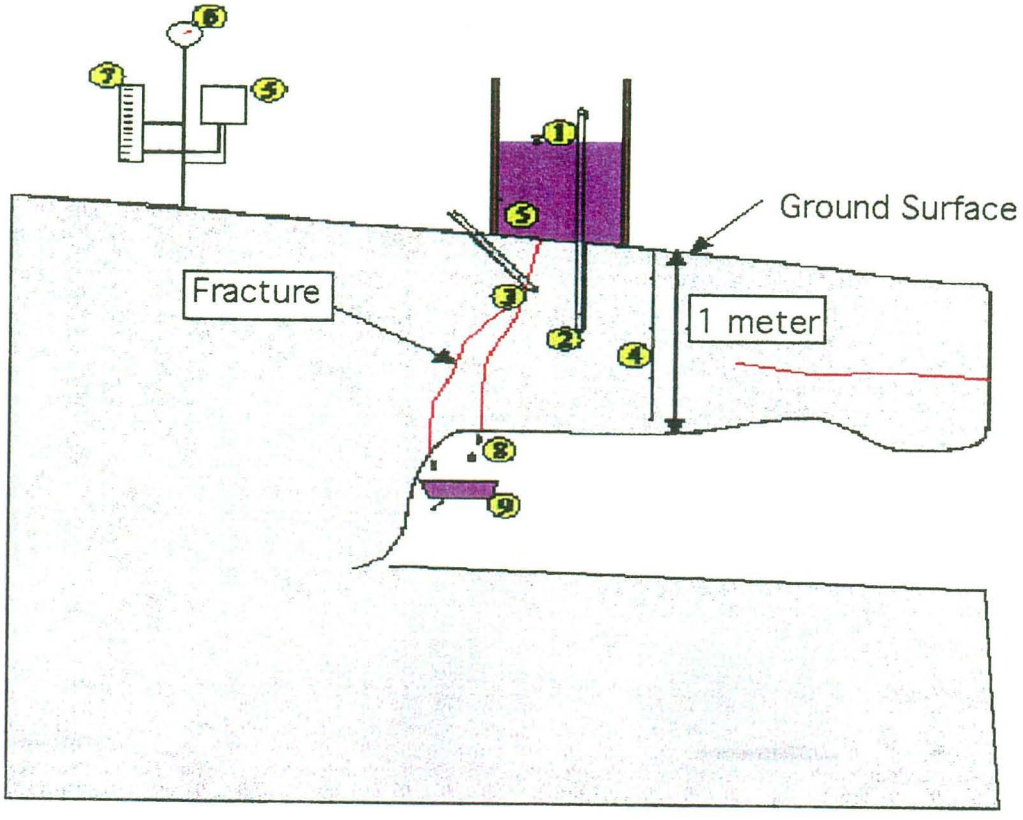

Figure 8. Design of a small-scale infiltration test at the Hell's Acre site in Idaho and the types of measurements conducted: 1-Water level and infiltration rate in the water gallery, 2-Basalt-matrix water pressure using tensiometers, 3-Fracture-matrix water pressure using tensiometers, 4-Temperature of rocks, 5-Ambient air and water temperature, 6-Barometric pressure, 7-Precipitation, 8-Outflow drip intervals, and 9-Outflow volumetric flow rate in 20x30 cm pans.

following parameters: water head in the infiltration pond, water and rock temperature, tensiometric pressures at 14 locations, barometric pressures, infiltration rates, and outflow rates as water drip intervals from 20 points and as volume from 12 locations on the underside of the outcrop. The design of this test allowed us to investigate the flow processes for elemental and small-scale components. The water dripping rates, or time intervals between drip events, can be used to characterize the elemental components. The area below the fracture is covered with a grid of 20 x 30 cm pans, which are used to collect the water drips from the fracture. Each pan collected one or more drips, combining several elemental components, averaging the outflow rate from the area above it. The water is routed from the pans to bottles attached to load cells to measure the outflow. The outflow rates determined from the pans can be used to characterize the small-scale components.

During infiltration experiments, the upper boundary condition was a constant water level in the surface pond. The infiltration tests were run for 1 to 18 days. The drainage periods between infiltration tests lasted up to several weeks to allow for sufficient drying of the fracture space. Successive tests started when the water pressure in the rock was approximately -100 mBars. We can assume that under this pressure the fractures were dry, and the matrix was partially desaturated.

6.2. Test Results and Conceptual Model of Flow on a Small Scale

We assume that the drip rates collected during these tests can be used to characterize the elemental components, while the infiltration and volumetric outflow rates combined with the tensiometric pressures can be used to characterize small-scale components. In order to provide a general understanding of the flow processes, we begin with the analysis of data obtained using the infiltration and volumetric outflow rates. Typical plots of the time variations in the volumetric infiltration rate and outflow rates at five locations along the fracture on the underside of the outcrop are shown in Figures 9a and 9b. We subdivided the time of the experiment into two periods (as shown in these figures).

Period 1. Immediately following the beginning of flooding, the infiltration rate increases due to the quick saturation of fractures and initially high water imbibition into the dry basalt. As water imbibes into the porous matrix, air is presumably pushed out into the surrounding fractures. In fractures, air becomes entrapped in the low aperture zones, thus blocking some flow pathways. This blockage leads to an overall decrease in the hydraulic conductivity of rocks and, consequently, to the decrease in both infiltration and outflow rates to minimum values at the time from 50 to 100 hours (Figures 9a and 9b). Figure 9b shows that the outflow rates become nearly the same at all observation locations. At this time, the water pressure measured in the fracture and matrix is practically the same (Figure 9c, tensiometers 2,4, and 5), which indicates no flow

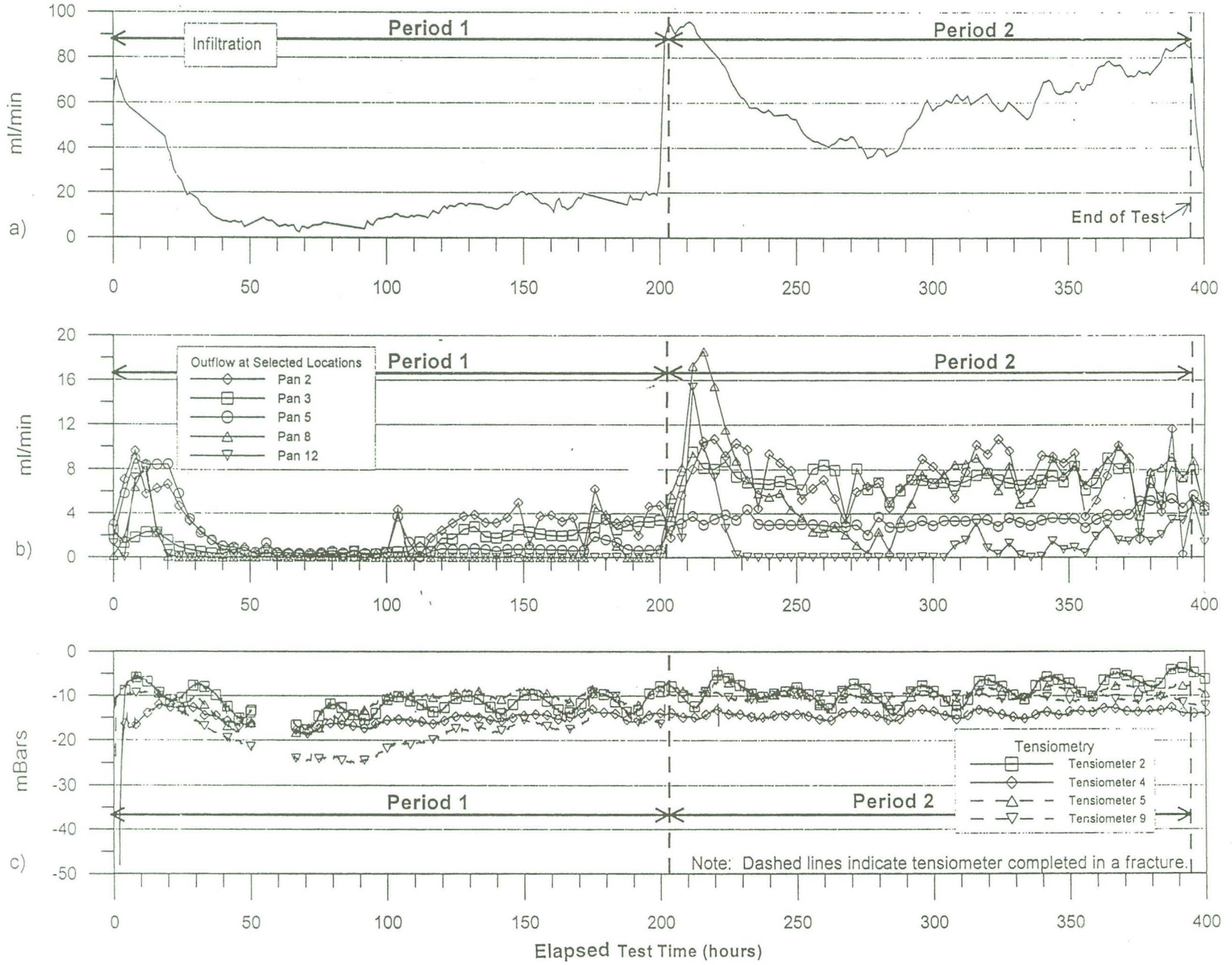

Figure 9. Results of a small-scale infiltration test: (a) Infiltration rate, (b) Outflow rates in several pans, and (c) Tensiometer pressure.

between the fracture and matrix. Note that tensiometer 9, which is located outside the footprint of the infiltration gallery, also showed a decrease in water pressure.

Subsequently, the flow rate increases, presumably as entrapped air dissolves into moving water and is removed in both free and dissolved phases. An identical flow behavior was observed in soils in the presence of entrapped air (Faybishenko, 1995). Comparison of Figures 9a and 9b shows that during Period 1, the trend and magnitude of the volumetric outflow rates are different from those of the infiltration rate. The simultaneous increase in the flow rates and tensiometric pressure (Figure 9c) supports the hypothesis of increasing rock saturation. The flow rates increased until the saturation reached a critical value, and most likely some flow paths were opened, at which time the flow rate increased drastically. This change is shown in Figure 9a as a boundary between Periods 1 and 2.

Period 2. During Period 2, the pattern of the infiltration rate is identical to that of the volumetric outflow rates for Locations 2, 3, and 8. This correspondence indicates a direct hydraulic connection between the surface pond and these locations. The trend of the outflow rates for Locations 8 and 12 is different because they are situated outside of the footprint of the pond. The magnitude of the flow rate increase at different locations along the fracture is quite varied and is accompanied by significant high frequency flow-rate fluctuations.

In general, it can be seen that small variations in the minimum values of the flow rate (between the time from 50 to 100 hours during Period 1) may lead to a wide range of flow rates thereafter. This shows that flow is quite unstable in time and space. The cumulative outflow through fractures was about 60% of the cumulative inflow, indicating that the remainder was presumably imbibed into the matrix, trapped in dead-end fractures, or lost to evaporation.

Figure 9c shows that despite an initial rapid increase in the flow during Period 2, the trend of the increase of tensiometric pressure remained essentially the same as that during Period 1. This indicates that the saturation of the matrix continued with time, but rocks were not fully saturated. It is important to note that tensiometers are not able to reflect rapid, high-frequency fluctuations, which were observed for the flow rate. Furthermore, under field conditions tensiometers may not detect a positive water pressure, which is likely to develop in fractures under ponded conditions. This condition occurs because the porous tip of the tensiometer averages the pressure over the volume of the tensiometer (Finsterle and Faybishenko, 1998), which includes both fracture and the adjacent unsaturated rock matrix, contributing to a negative capillary pressure. Despite these limitations, the water pressure trends (Figure 9c), combined with the flow rate data (Figures 9a and 9b), indicate: (1) a rapid fracture saturation just after the beginning of flooding, (2) water imbibition into the matrix, and (3) water flow through fractures.

An analysis of the results of water dripping observed at one of the drip points, Drip Point 6, is shown in Figure 10. A random-looking time variation of water-drip intervals is shown in Figure 10a. The analysis of these data showed that the optimum time delay $\tau = 3$, and the dimension needed to unfold the attractor is $n = 5$. Figure 10b shows a three-dimensional attractor that has a definite structure. The spread of points on the attractor reveals the presence of a combination of both chaotic and random components for the frequency of water dripping from a fracture.

7. Intermediate-Scale Infiltration Test at the Box Canyon Site

7.1. Test Design

The field investigation at the Box Canyon site was conducted in order to develop a conceptual model of the geometry and physics of flow and transport at the intermediate scale. We investigated a fracture pattern at the Box Canyon outcrop and conducted a series of ponded infiltration tests at the center of the basalt flow about 30 m away from the outcrop exposure (Faybishenko et al., 1998b; 1999). Because the spacing between the largest basalt column bounding fractures (which corresponds to the diameter of largest basalt columns) is as large as 4 - 4.5 m, we constructed a 7 x 8 m pond. We assumed that all types of fractures exist beneath the pond, including at least a few fractures transecting the entire basalt flow. Monitoring of water flow and tracer transport was conducted in 38 vertical and slanted boreholes, which were instrumented using tensiometers, suction lysimeters, electrical resistivity (ER) probes, time domain reflectometry (TDR) probes, and thermistors. Water-content distribution was determined using neutron logging, ground penetrating radar, and ER tomography.

7.2. Conceptual Model of the Geometry of the Fracture Pattern

Figure 11 shows a map of the Box Canyon outcrop. In the upper ~2/3 of the flow thickness, the joint spacing increases with depth. The base of the basalt flow shows an inverted fracture pattern, in which the lower basalt contact contains smaller fracture spacing than in the center of the flow. At the exposed upper surface, the spacing is as small as 0.3 - 0.5 meters. The upper 2/3 of the basalt flow has more fractures than the lower 1/3. In some basalt flows, a region near the center of the flow contains highly fractured rock that does not display the typical columnar structure (Long and Wood, 1986; Tomkeieff, 1940). The fracture map shown in Figure 11 illustrates that the central fracture zone is observed below the infiltration site.

The map shown in Figure 11 was used to construct a 2D conceptual model of the geometry of the fracture pattern (Figure 12). This model is based on the assumption that

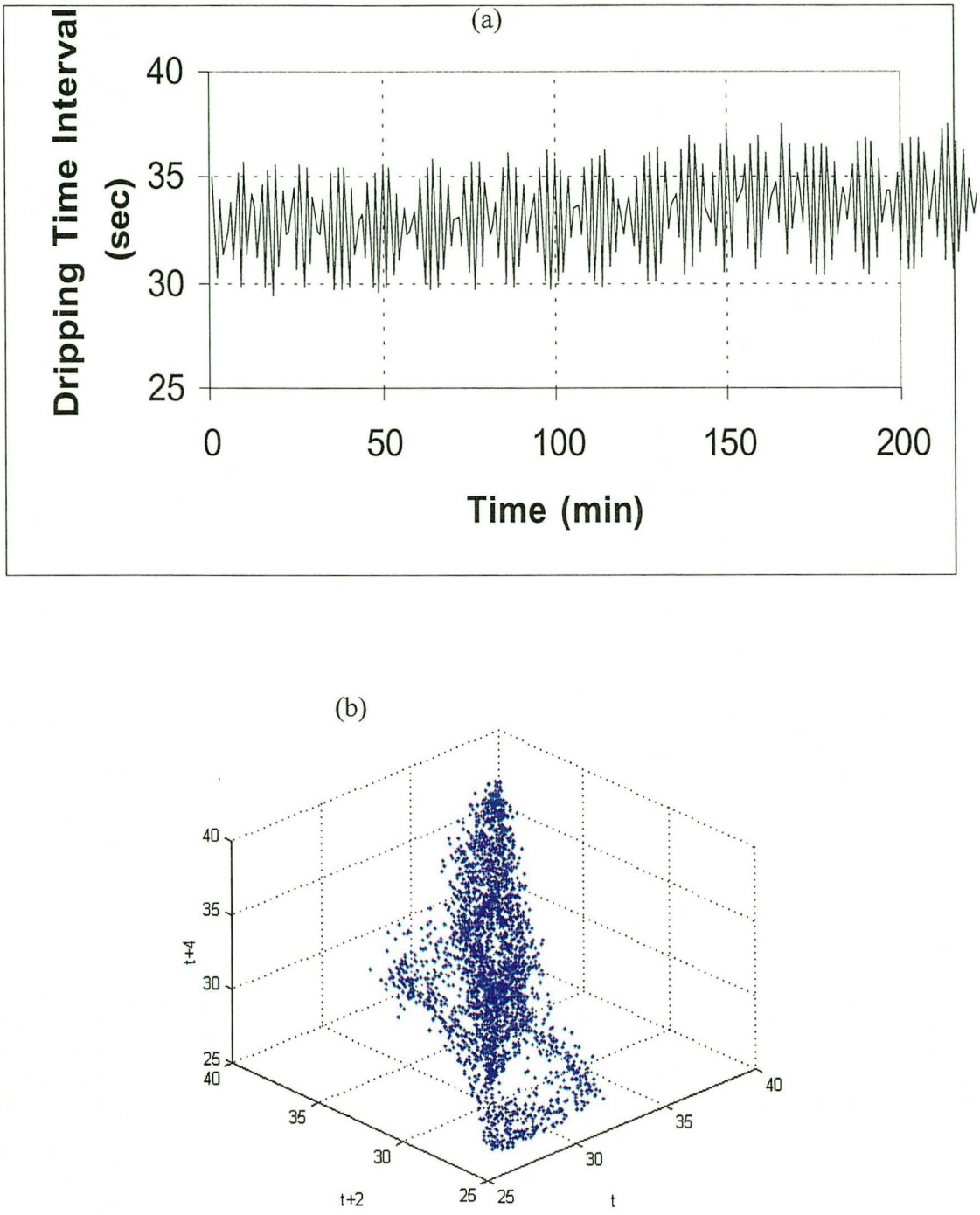

Figure 10. Variations of time-intervals of water dripping: (a) time-series data (only first 200 points are shown), (b) a 2D attractor using τ=3, which was plotted using 2,000 points.

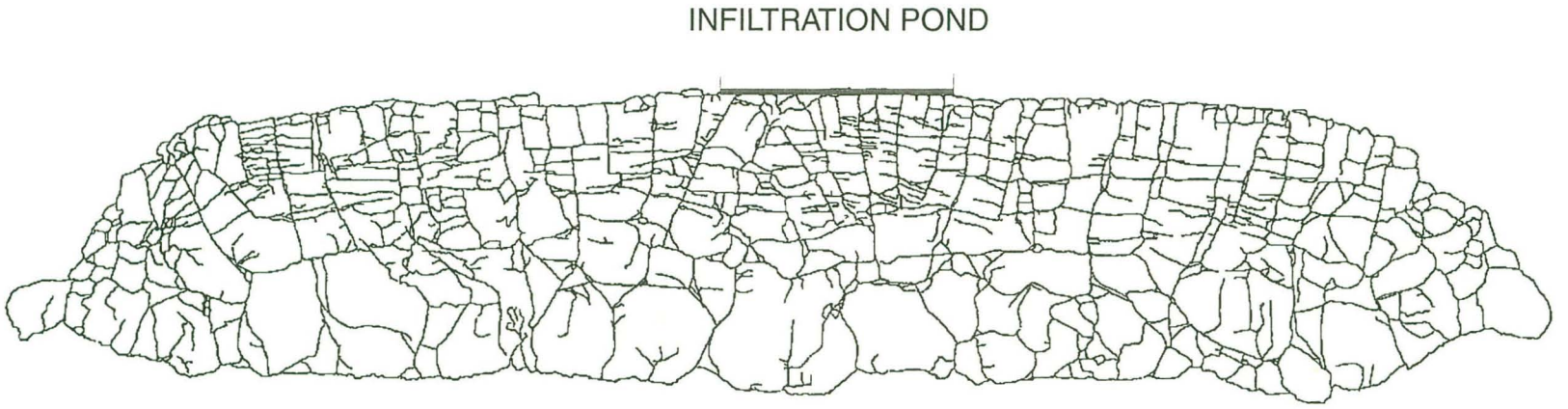

Figure 11. Fracture map of basalt flow outcrop at the Box Canyon Site located about 30 m from the research site. Figure shows that the width of the infiltration pond was about twice as much as the width of the largest basalt columns. The fracture map was prepared by J. Lore (Stanford University).

there are four generations of vertical column-bounding fractures. Starting from the surface, the two smallest basalt columns of size n (1st generation) merge into a column of size $2n$ (2nd generation). Below this, two columns of size 2 n merge into a column of size $4n$ (3rd generation), and then two columns of size $4n$ merge into a column of the size $8n$ (4th generation). Visual inspection of several basalt outcrops in the field showed that every set of vertical fractures is connected through horizontal vesicular layers and fractures, which are included in the model as well. In addition, Figure 12 shows the presence of some dead-end, or nonconductive, fractures. However, at this time we do not have a quantitative evaluation of dead-end fracture spatial distribution.

The tree-type model of the fracture pattern described above implies that a small variation in initial conditions and properties of the fracture network, particularly, at fracture intersections, can lead to significant divergence of flow paths within the basalt flow. In other words, two nearby particle trajectories initiated from slightly different initial locations may not stay close to each other over time. They may diverge and follow entirely different paths, which directly leads to limitations in predicting flow behavior.

7.3. Conceptual Model of Flow

Field Observations. During flooding of the surface, the upper 30-60 cm of vesicular, highly weathered basalt behaves more or less like a uniformly saturated, porous medium. A series of infiltration tests (Faybishenko et al., 1999) showed that the infiltration rate into the subsurface decreased with time exponentially according to Horton's model (Horton, 1940). The near-surface basalt is supposed to be subject to sealing by biofilms, soil particles, and entrapped air that can reduce the fracture and matrix permeability. As the infiltration flux decreases, the fractures below 30-60 cm, which were saturated at the beginning of flooding, may thereafter become desaturated.

Because of the complexity of the fracture network, it is possible to have the effects of both divergence and convergence of flow paths in different parts of the basalt flow.
An important factor affecting water flow in basalt is a funneling effect that develops as a result of the convergence of the flow paths caused by the decrease in the number of conducting fractures with depth. At the same time, drastic variations in permeability of fractures and matrix create a significant divergence of flow paths and a significant dispersivity effect for chemical transport. This process decreases the tracer concentration in the rubble zone, which was determined during the infiltration tests at Box Canyon (Faybishenko et al., 1999). We assume that dead-end fractures may accumulate contaminants, which will diffuse over time into the matrix. However, it is impossible to identify *a priori* which fractures will transmit water and contaminants during an infiltration test.

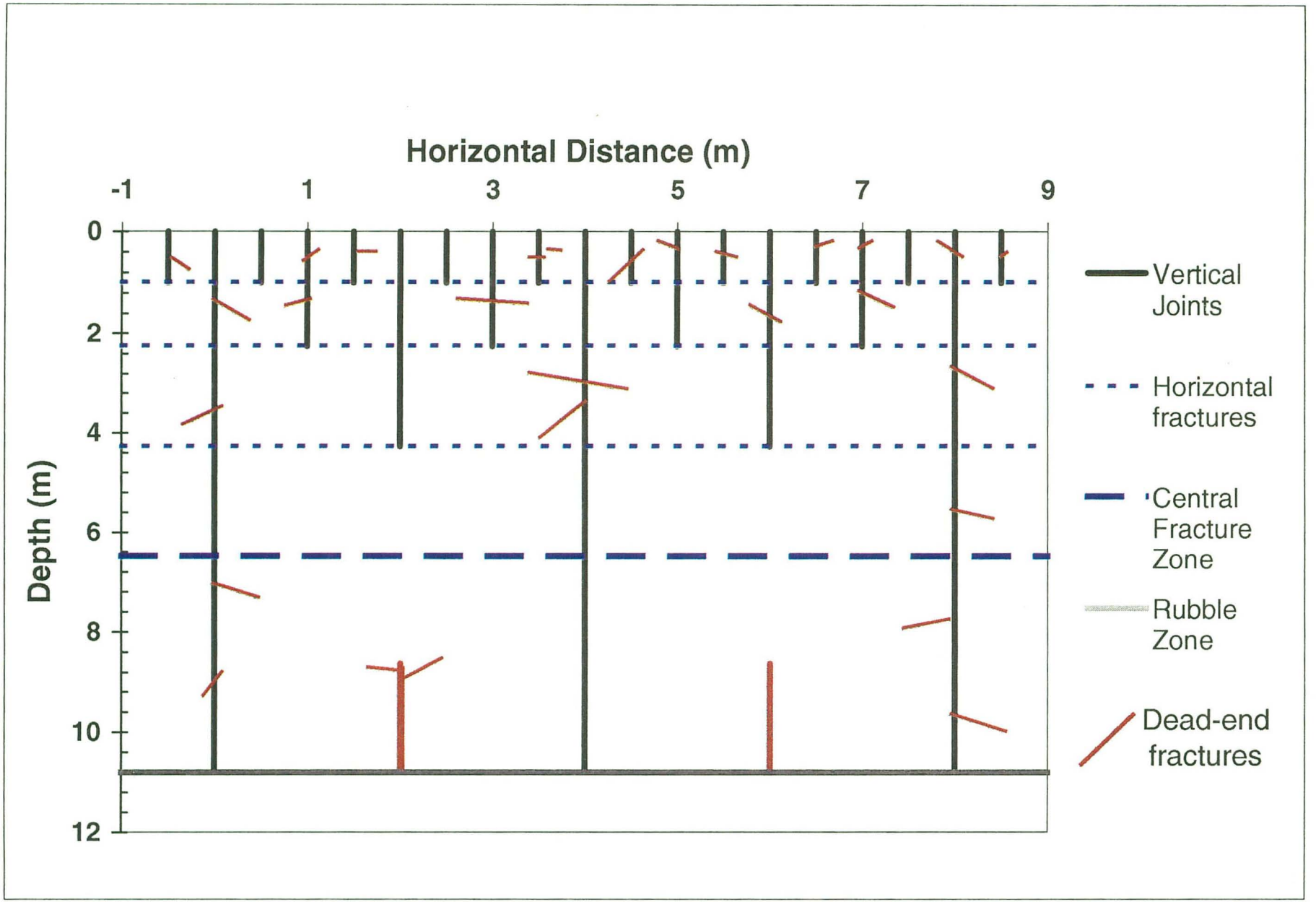

Figure 12. A conceptual model of the fracture pattern showing the vertical and horizontal fractures and fracture zones, as well as dead-end fractures. The locations of dead-end fractures are arbitrary.

A complex geometry of flow was observed using the GPR survey. Figure13 shows an example of the radar velocities between two boreholes located four meters apart just outside the pond. This figure also shows generalized lithological and fracture logs of these wells. The red color indicates a low radar velocity associated with higher moisture content, and the blue color indicates a higher velocity as affected by lower moisture content. This could indicate either drier conditions or lower porosity in the rocks. This figure shows three horizontal low-velocity zones, presumably wetted zones, located in vesicular basalt and the central fracture zone. We hypothesize that subvertical column-bounding fractures connect these horizontal zones and extend below them to the underlying rubble zone. Unfortunately, individual fractures cannot be resolved by the GPR tomograms because of the small volume of the fractures. Assuming an aperture of 1 mm and a fracture spacing of 2 m, the effective fracture porosity is 1 mm/2 m = 0.0005, which is quite small compared to the matrix porosity (~5%). Therefore, we cannot expect such small fractures to show up on the tomogram, even though they are main conduits for water flow.

Field investigations showed that because the number of probes is limited, the results of measurements are usually incomplete and are significantly dependent on the type of instrumentation. For example, tensiometers, ER and TDR provide "point"-type, passive measurements within the length of the sensors, which is usually 5-20 cm, and they detect water only if water contacts the probe (Figure 14). Neutron logging of the moisture content and water sampling with suction lysimeters provide small-scale, near-borehole measurements within distances of 30-40 cm from the borehole. The cross-borehole radar tomography and electrical resistivity tomography measurements, which are effective within a distance of 2-4 m, can provide important information on the relative moisture content within fractured zones, but the resolution cannot provide information about flow in individual fractures. Because the information about the flow processes provided by field measurements is limited, we complemented the field data with mathematical modeling to investigate flow and chemical transport.

Modeling of Water Flow and Tracer Breakthrough Curves. We generated a relatively simple 2D numerical model using the numerical simulator TOUGH2 (Pruess, 1987; 1991) to simulate water flow and conservative tracer migration underneath the Box Canyon pond (Doughty, 1998). We created a vertical cross-section model of 20 x 20 m in extent, using a regular rectangular grid with a 0.5-m grid spacing (as shown in Figure 15a). The flow properties of the model were assigned using a deterministic approach designed to approximately duplicate the fracture pattern and types of rocks observed at the Box Canyon cliff face (Figure 11). Gridblocks representing vertical fractures are assigned high vertical permeability to allow preferential flow through the fracture, low horizontal permeability to limit fracture-matrix flow, and small porosity to account for the small aperture of the fracture. For gridblocks representing horizontal fractures, the assignment of horizontal and vertical permeability is reversed.

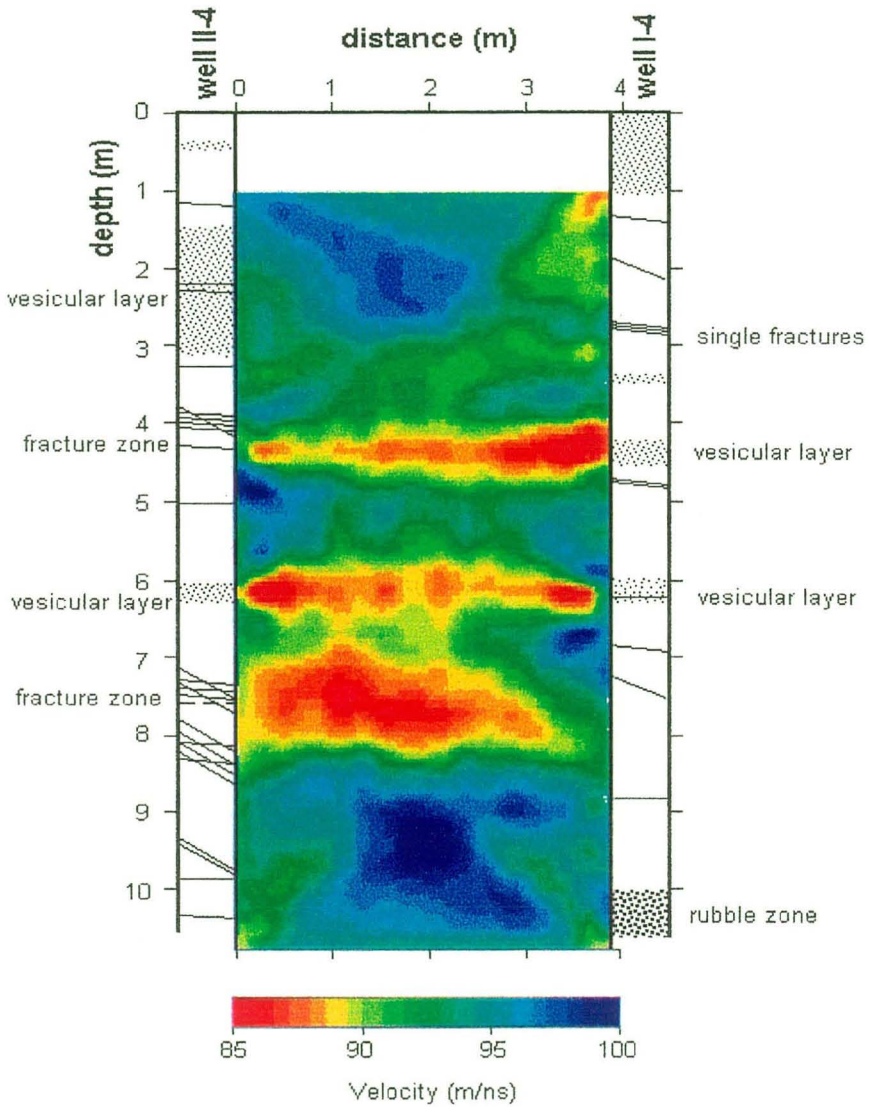

Figure 13. An example of the radar velocities between two boreholes located four meters apart just outside the pond. The red color indicates low radar velocity zones associated with a higher moisture content, and the blue color indicates higher velocity zones with a lower moisture content. The field data were taken in October 1998 by K.H. Williams, and the data inversion was conducted by J. Peterson of LBNL.

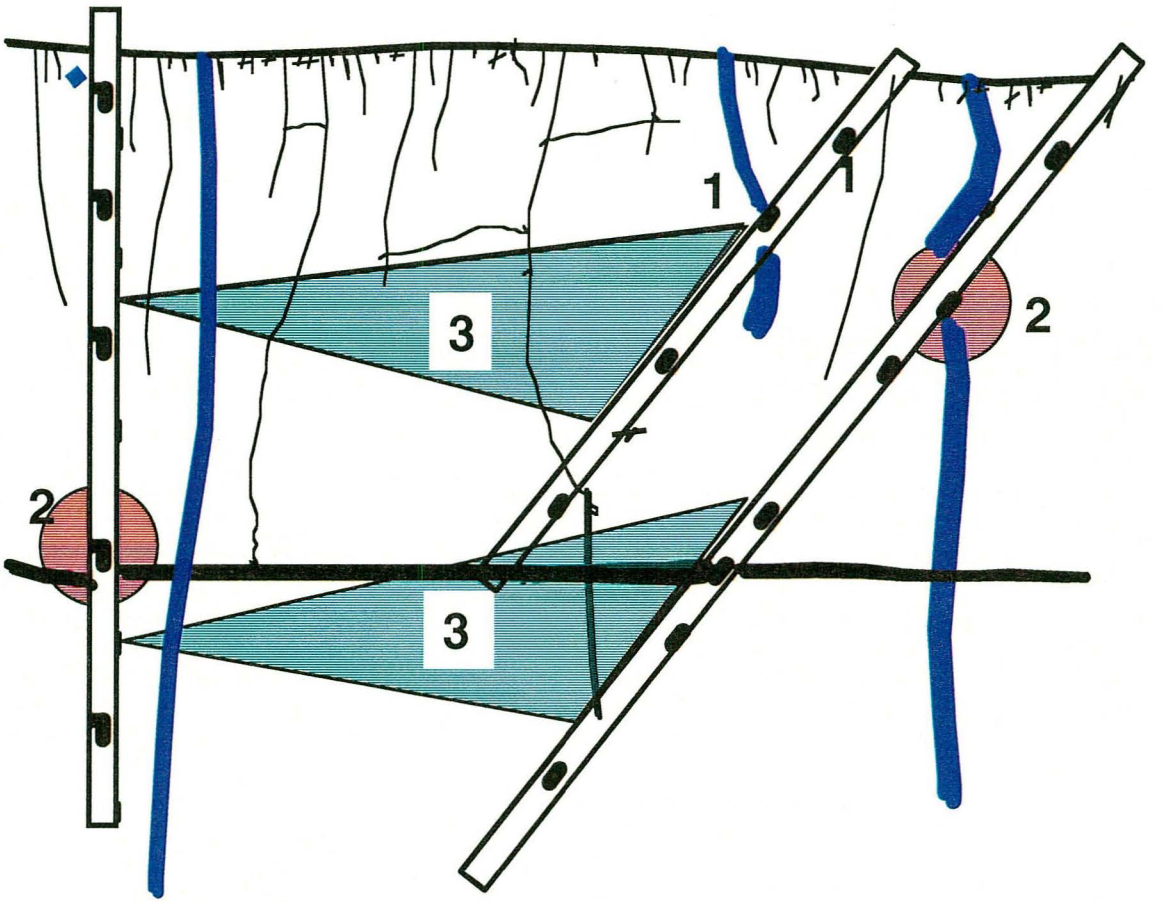

Figure 14. Schematic presentation of types of measurements in fractured rocks using: 1- Point-type, passive probes (tensiometers, ER and TDR) of a 5-20 cm size, which detect water only if water contacts the probe; 2- Near-borehole moisture content measurements using neutron logging, and water sampling using suction lysimeters within the distance of 30-40 cm from the borehole; and 3- Cross-borehole radar and 3D ER tomography on the distance up to 10-12 m.

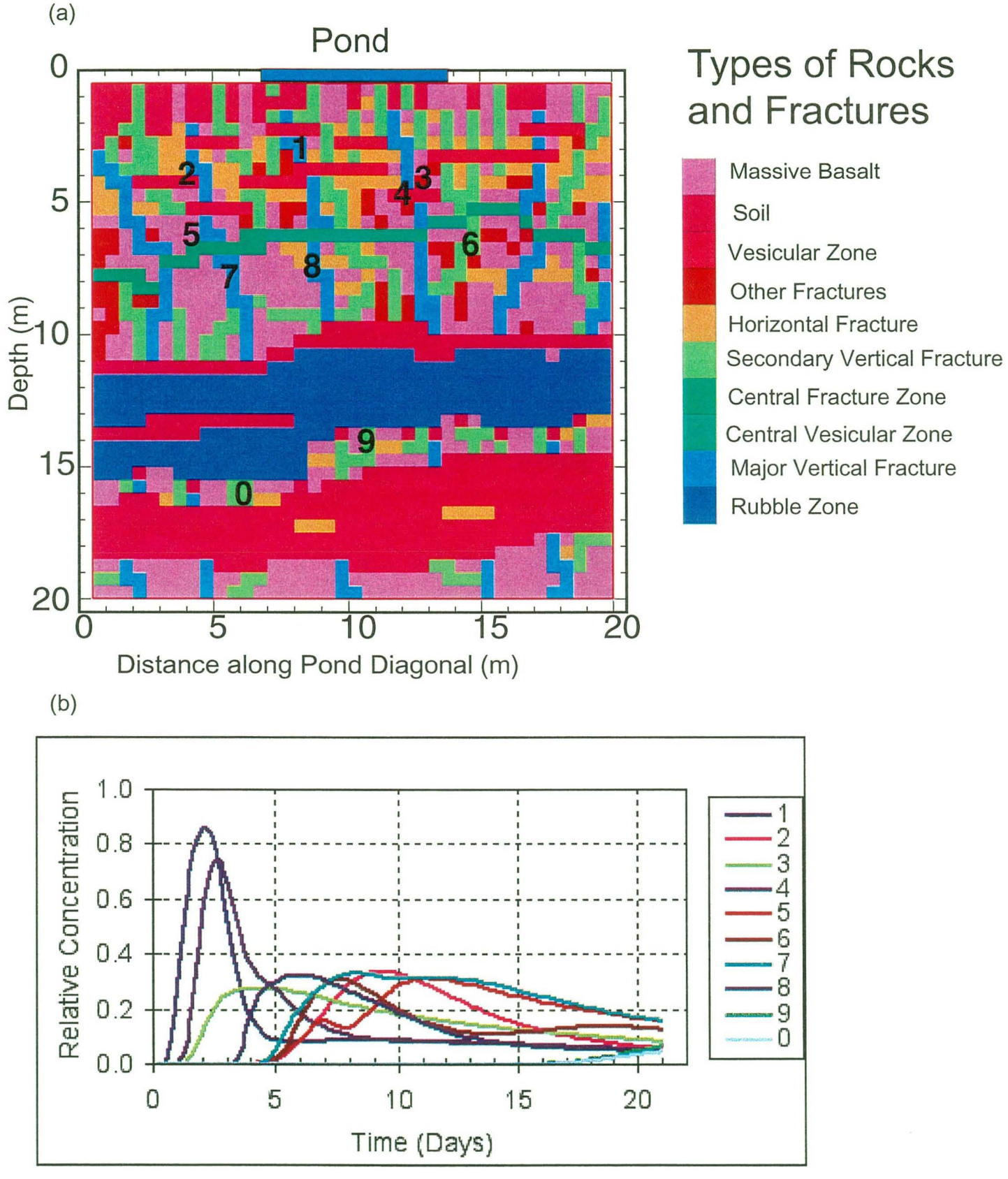

Figure 15. The geometry and types of rocks (a) used for the 2-D modeling of Box Canyon infiltration test, and breakthrough curves (b) obtained for different locations. Location numbers on figure (a) correspond to numbers of breakthrough curves on figure (b).

Processes modeled included water and air flow, as well as transport of a conservative liquid tracer. The pond is treated as a constant head and concentration boundary. Figure 15a shows the locations of the monitoring points for tracer breakthrough curves (BTCs). Figure 15b shows a wide range in the behavior of the BTCs. For example, Curves 1 and 4 show sharp peaks, suggesting strongly preferential flow with a small fracture-matrix interaction. Curves 2, 3, 5, and 7 show long tails, suggesting significant matrix diffusion. Curves 4, 5, 6, and 7 show double humps, suggesting a convergence of multiple flow paths. This modeling of breakthrough curves thus confirms the notion that fracture network geometry, along with the type of rocks in which the fractures are imbedded, determines the overall pattern of flow and transport. Results from the modeling of moisture changes (Doughty, 1998) are consistent with field observations and show that vertical preferential flows occur primarily along the column-bounding fractures. A slower imbibition occurs into the surrounding rock matrix. Layers and lenses of vesicular basalt, the central fracture zone, and the rubble zone provide conduits for lateral flow of both water and air, resulting in the wide variety of BTCs seen in Figure 15b. The character of the BTCs does not show a correlation to the depth or lithology of the monitoring point. Rather, the BTCs are dependent on the overall geometry of the fracture pattern, including the fractures above and below the monitoring location.

Summary of the conceptual model of flow. The deterministic-chaotic nature of the intra-basalt flow fracture pattern and the chaotic nature of flow processes discovered on the elemental and small scales support the hypothesis that flow and transport in basalt at the intermediate-scale can also be chaotic. At the same time, the limited number of single-point probes usually available to monitor intermediate scale field experiments cannot be expected to explicitly reveal spatially chaotic flow characteristics, which may occur as a result of a fractal flow-path structure (Barton and Larsen, 1985; Cox and Wang, 1993; Fedder and Jossang, 1995; Hardy and Beier, 1994). Furthermore, for the observations at the intermediate scale, processes all along the flow path from the pond to the monitoring point affect behavior, leading to higher attractor dimensions and precluding unequivocal identification of chaos in time-series data. Therefore, we believe that the optimal way to analyze the field monitoring data is to simulate the geometry of the fracture pattern with deterministic models (such as those shown in Figures 12 and Figure 15a), along with stochastic models of hydraulic parameters (Mantoglou and Gelhar, 1987a,b; Yeh et al., 1985) for the different types of fractures and rocks.

8. Large-Scale Infiltration Test at the Radioactive Waste Management Complex

8.1. Test Design

The LSIT, which was conducted south of the RWMC at the INEEL, was probably the largest infiltration test ever conducted in the U.S. It was designed to assess flow and

transport phenomena at the scale of several basalt flows, separated by rubble zones, between the surface and a sedimentary interbed at a depth of 55 m. An area of approximately 26,000 m^2 was flooded for a month using water that was pumped from the underlying Eastern Snake River Plain aquifer and then was piped into the 183 m diameter infiltration basin. After 6 days of flooding, several short-lived radioactive tracers, as well as a NaBr tracer, were added to the infiltration basin. The total volume of water supplied into the pond was 134 million liters. After mixing was accomplished, no new water was added to the basin for 11 days while the tracer pulse infiltrated. The total duration of the infiltration test was 7 months. Subsurface migration of infiltrating water and tracers was monitored by several techniques (as described below).

The monitoring well network consisted of 70 wells, as shown in Figure 16. Given the heterogeneous nature of the fractured vadose zone, it was anticipated to detect preferential flow and lateral spreading of water along rubble zones, as well as the formation of perched water bodies above the sedimentary interbeds (Hubbell, 1990). The arrangement of wells within 100 m of the infiltration basin (in and around the infiltration basin) allowed for the monitoring of water and tracers flowing vertically beneath and laterally away from the infiltration basin. Monitoring for the subsurface water movement began immediately after the beginning of flooding using multiple monitoring systems. The following types of data were collected: (a) neutron logging to determine the changes in the moisture content of rocks in the near vicinity of the monitoring wells, (b) gamma spectroscopy to track the movement of the gamma-emitting radioactive tracers, (c) water sampling to determine the water appearance and tracer breakthrough curves, and (d) perched water level measurements.

8.2. Test Results and Conceptual Model of Flow

Despite the expectation of lateral flow, no water or tracer was observed in boreholes beyond the footprint of the infiltration pond except for perched water that formed on top of the sedimentary interbed at a depth of 70 m. The perched water moved down the slope of the interbed through a widespread rubble zone immediately above the low permeable sedimentary interbed. The fact that infiltrating water was not observed in partially saturated fractured basalt outside the basin suggests high permeability of intra-basalt vertical fractures and rubble zones sufficient to transmit all water downward. Thus, the LSIT showed that in addition to the effect of an intra-basalt fracture pattern (studied at the intermediate-scale), we have to take into account the geometry and permeability of inter-basalt rubble zones. Furthermore, low-permeability sedimentary layers can create perched water zones that induce the lateral spread of water and contaminants.

Figure 17 shows the water arrival at different depths of the vadose zone, which was determined using neutron logging. This figure also includes the water arrival times into open boreholes screened at the depth of 55 m, indicating the incipient formation of

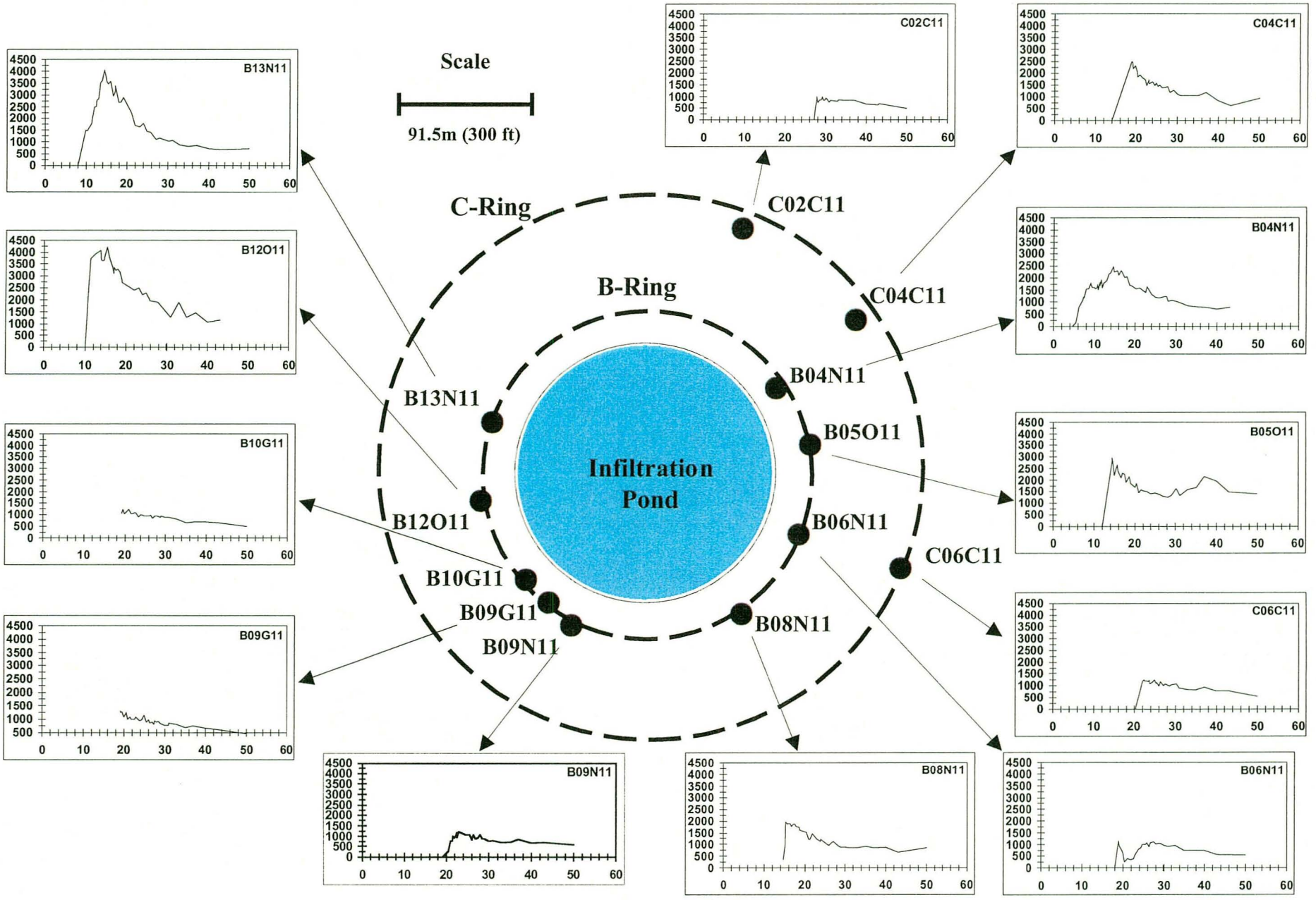

Figure 16. General layout of the infiltration pond and the borehole monitoring system during the LSIT, and breakthrough curves of Se-75 determined in boreholes screened in a perched water zone (vertical axis - Se-75 concentration in pCi/l, and horizontal axis - time in days since the tracer addition into the infiltration pond.

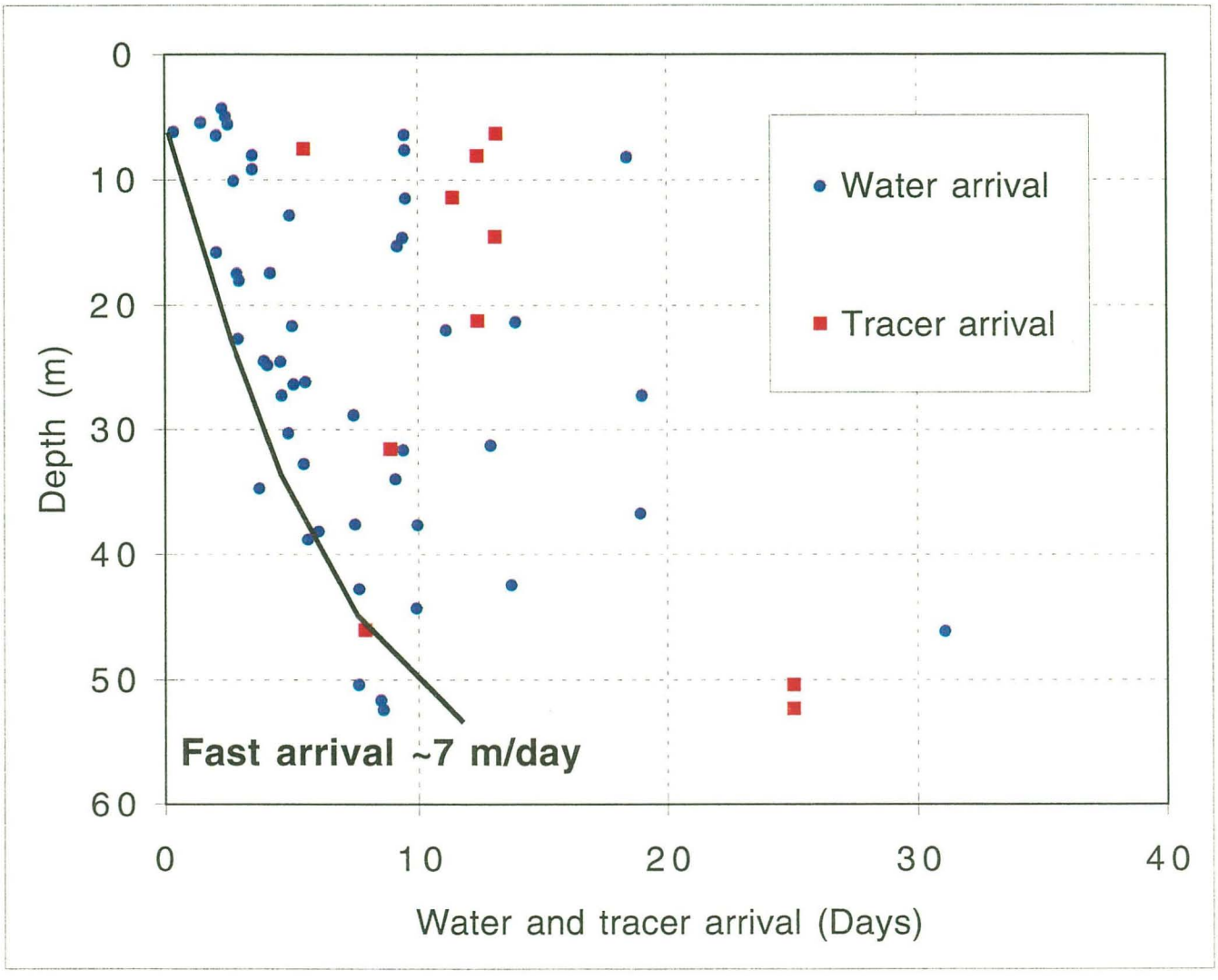

Figure 17.The relationship between the time of water arrival (determined from neutron logging) and the Se-75 tracer arrival (determined from water sampling) and depth.

perched waters. The left dashed line in Figure 17 shows the first water arrival at different depths. From this figure, the velocity of the downward distribution of the wetting zone is 7 m/day. Smaller scales of observation would have to consider local hydrogeologic features that may account for wide departures from the average wetting zone travel time of 5 m/day determined by Bishop and Porro (1995).

Despite adding tracer-free water to the infiltration basin for 6 days before the addition of tracers, the first water observed in several wells contained tracer. Also, tracer-free water was observed in several lysimeters throughout the course of the test. Intervals containing insufficient water for the collection of samples were observed between water bearing zones. Consequently, Figure 17 shows little correlation between the distance from the surface and tracer arrival time. Note that the BTCs that were determined using water sampling with suction lysimeters do not have unique interpretation because when vacuum is applied to collect water, water can be withdrawn from different rock volumes (depending on the moisture content and permeability of fractures and matrix).

Figure 18 illustrates a variety of tracer breakthrough curves observed at different locations during the LSIT. One can see a conventional BTC near the surface, multi-modal curves as affected by migration from different fractures, and no tracer detected at some points. Note that at some locations that became saturated quickly after the beginning of flooding, the tracer had not arrived after a month. This non-appearance can be attributed to changes of water-flow pathways over time. Water may flow into dead-end, nonconductive fractures easily, but because it cannot continue flowing out of the fractures, no subsequent tracer can flow into these fractures by advection. Tracer can enter these fractures only by diffusion or flow through the surrounding basalt, both of which are likely slow processes. Thus, a combination of the water and tracer experiments can be used to identify zones of preferential flow and locations of dead-end, nonconductive fractures.

9. Discussion

The complex geometry of basalt flows and intra-basalt fracture networks that have wide variations in the permeability of dense basalt and highly fractured rubble zones have raised concerns over how water flow and contaminant transport in such systems should be characterized. Because of geological and hydrogeological complexity, as well as uncertainty of measurements, a hierarchy of scales, methods, and models should be used to characterize flow and transport phenomena in fractured basalt.

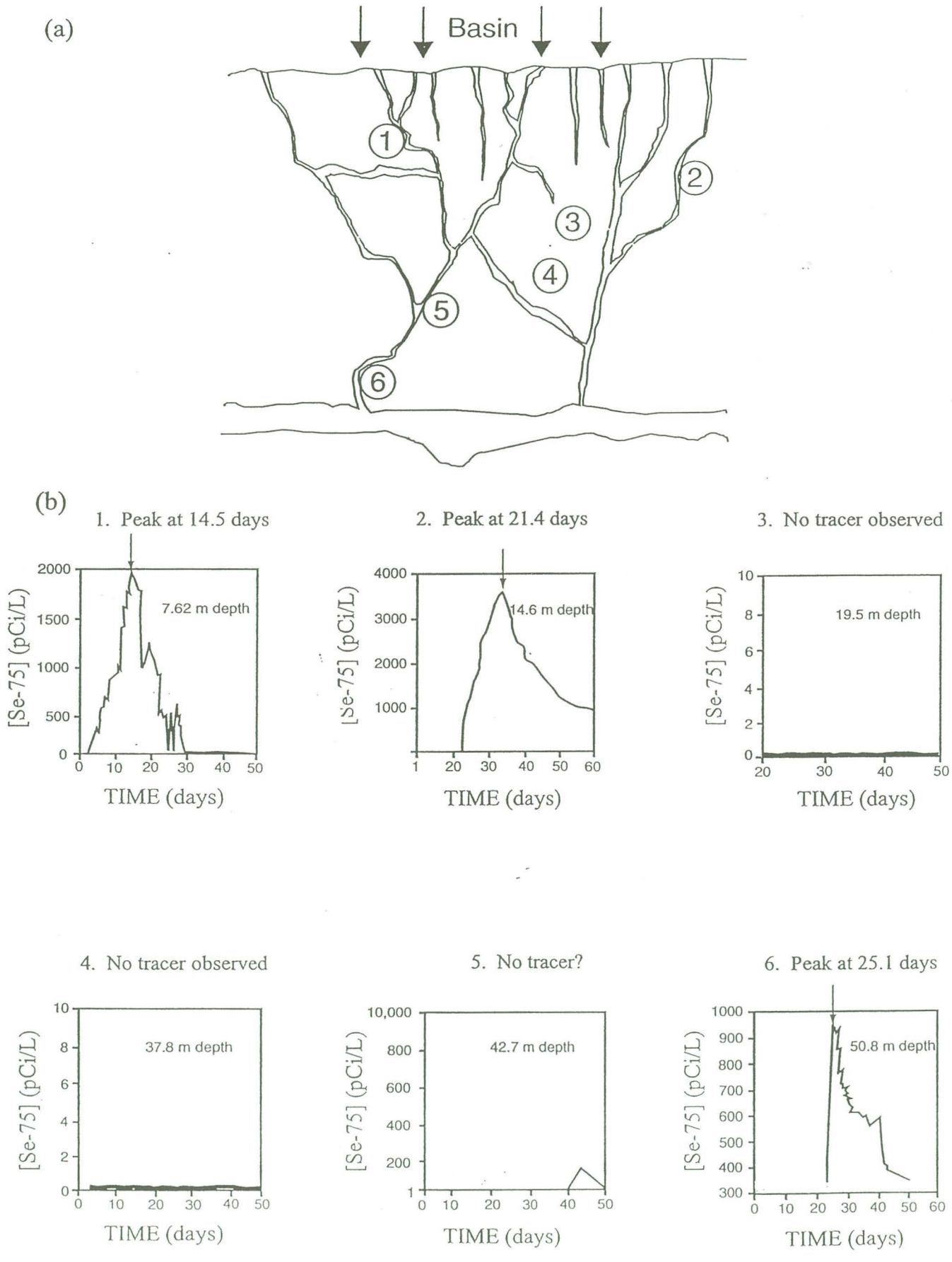

Figure 18. A conceptual model (a) of the fracture pattern and corresponding breakthrough curves (b) for Se-75 for several locations shown on the conceptual model in figure (a).

Elemental scale investigations are conducted to study in detail the physical nature of spatial and temporal characteristics of flow processes in a single fracture or a block of the basalt matrix, using small laboratory cores, fracture replicas, or point-size measurements under field conditions. The size of measurements is from a few centimeters to 10-20 cm. Laboratory investigations of flow in a single fracture of basalt showed the phenomenon of film flow (Tokunaga and Wan, 1996) as well as water channeling and meandering along narrow pathways on the fracture surface (Su et al., 1998). Laboratory experiments using capillary tubes inserted into fracture replicas showed that water does not flow uniformly along a fracture surface, but intermittent flow and water dripping occur along flow channels. The water dripping and meandering within the fracture generates nonperiodic fluctuations of water pressure, which are not stochastic in nature. The pressure fluctuations can be described using deterministic-chaotic models with a certain stochastic component that is not a dominant factor controlling the system behavior. The results of studies on the elemental level can be used to better understand water dripping from a fracture under field conditions in boreholes, tunnels, caves, and other underground openings. However, laboratory studies of fractured rocks have certain limitations, because we cannot determine how to combine the individual processes for characterizing the total system.

Small-scale investigations involve a volume of rock within a single basalt flow with one or a few fractures over an areal extent of approximately 0.5-1 m^2. Field experiments on this scale conducted by Nativ et al. (1995) and at the Hell's Half Acre site (Podgorney et al., 1997; 1999) confirmed that fracture flow is in fact occurring as dripping phenomena. Figure 19 illustrates a conceptual model of water flow through a block of fractured basalt that occurs as dripping phenomena from many locations along the fracture. These locations are not stable with time and are meandering. The intervals of water dripping from a single location can be described using a chaotic model with some random component. At the same time, the volumetric outflow rates combined from several dripping locations exhibit spatial and temporal instability, with primary low frequency fluctuations and secondary high-frequency fluctuations. The fracture-matrix water interaction and entrapped air (Persoff and Pruess, 1995) are presumably the main new factors affecting the spatial and temporal flow instability compared to the elemental scale, which were also identified in several studies (Glass et al., 1991; Lenormand and Zarcone, 1989; Nicholl et al., 1993).

With the increasing scale of field investigation, the combination of many degrees of freedom may lead to attractors of such high dimension that the overall behavior of the system does in fact look stochastic (despite its deterministic chaotic nature on the elemental scale). Contrary to laboratory conditions, water pressure cannot be measured so precisely under field conditions because single tensiometers, conventionally used to measure the water pressure, provide volume-averaged pressure measurements within the volume of the tensiometer porous cup (Finsterle and Faybishenko, 1997). Thus the averaged pressure does not exhibit high-frequency fluctuations that actually take place on

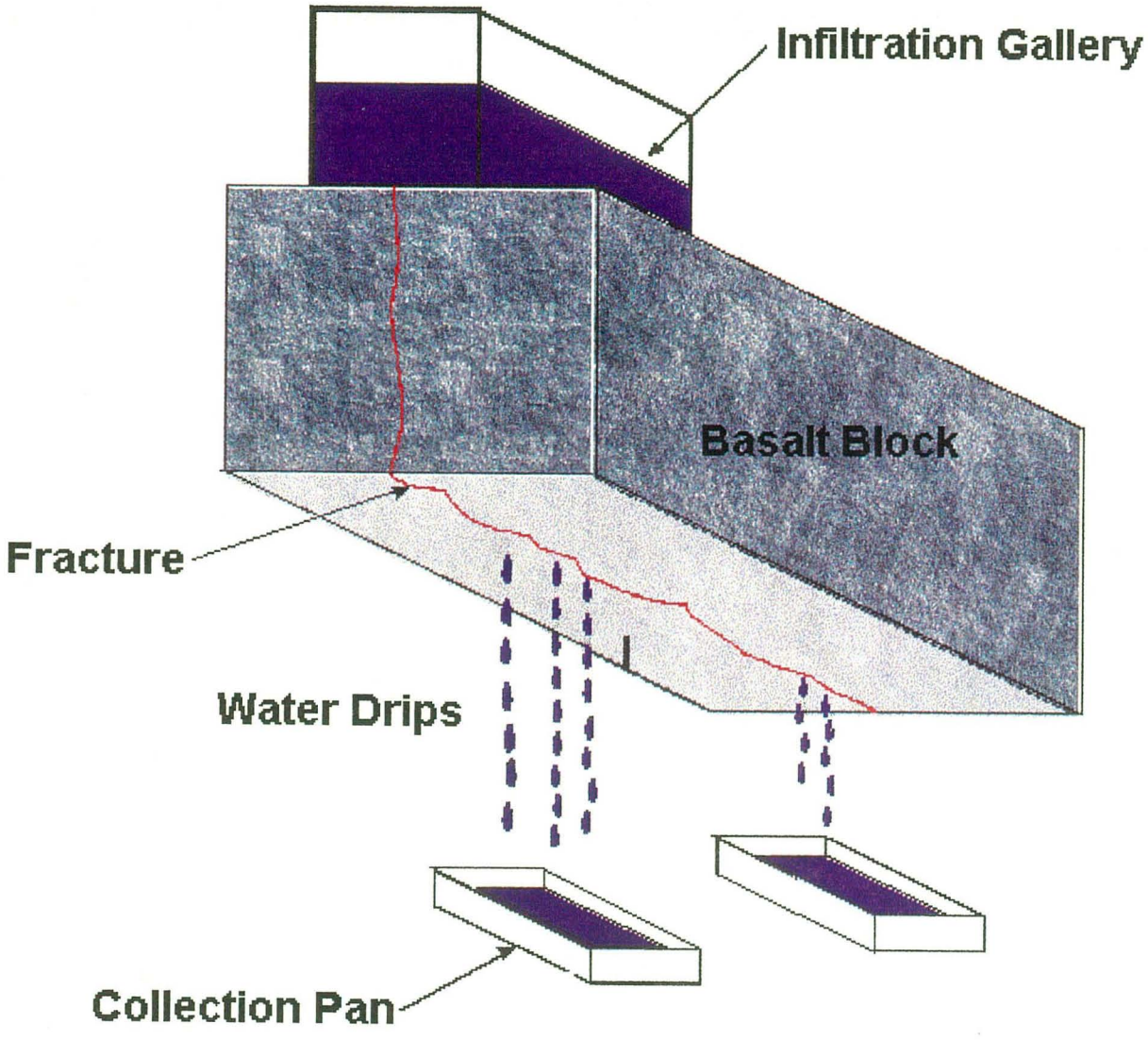

Figure 19. A conceptual model of a field infiltration test showing water dripping, which can be considered as an elemental component, and a collection of water into pans that can be considered as a small-scale component.

account of water dripping, as observed in both the field and laboratory. In the meantime, the comparison of water pressure measured using tensiometers installed in the fracture and the matrix can be used to determine the general trend of the rock saturation and the relative roles of water flow through fractures and matrix. The most important practical application of small-scale investigations is the study of physics and models of flow taking into account the fracture-matrix interaction.

Intermediate-scale investigations are conducted within the volume of rock in a basalt flow involving the intra-basalt flow fracture-network over an areal extent of approximately 10-100 m^2. A series of ponded infiltration tests at the Box Canyon site showed that during flooding of the surface, the upper 30-60 cm of vesicular, highly weathered basalt acts more or less like a uniformly saturated porous medium. The infiltration rate decreases with time exponentially. The fractures that were saturated at the beginning of flooding may become desaturated thereafter. Important factors affecting the decrease in the infiltration rate into fractured basalt are plugging of the fractures by soil particles, biofilms, and entrapped air, as well as a funneling effect resulting from a convergence of flow paths as the number of conducting fractures decreases with depth. Vertical flow occurs through subvertical, column-bounding fractures, which interconnect the horizontal layers of vesicular basalt, the central fracture zone, and the rubble zone. These highly permeable zones provide conduits for lateral flow of both water and air and create a divergence of flow paths leading to a significant dispersivity for contaminant transport.

We assume that the presence of dead-end fractures, which may retain contaminants, will promote long-term diffusion of these materials into the matrix. Unfortunately, individual fractures cannot be resolved by existing field hydrogeological and geophysical methods, on account of the small volume of fractures. Because single probes can easily miss a zone of preferential flow, field measurements provide limited information about the flow processes. In this case, modeling is needed to investigate flow and chemical transport.

Modeling showed the importance of taking into account coupled processes of two-phase (water and air) flow (Doughty, 1998). Modeling also showed that different BTC behaviors exist reflecting strongly preferential flow with fracture-matrix interaction and suggesting the convergence of multiple flow paths. The BTC at a given location depends on the entire flow path from the pond to that location and is strongly affected by the overall geometry of the flow path and lithology along the fracture pattern.

The practical application of the intermediate-scale investigation is understanding the flow processes underneath single tanks like those at the RWMC in Idaho and at Hanford.

Large-scale investigations involve the volume of rock containing several basalt flows and the rubble zones between them over the area that usually exceeds 1,000 m^2. At this scale, we can study flow in the fracture networks and regional hydrogeological processes,

which are affected by the vertical and horizontal rubble zones, as well as sedimentary interbeds. A limited number of single probes that were available to monitor the LSIT cannot explicitly reveal all spatial and temporal flow characteristics of the vadose zone. However, the creation of the perched water zone above the sedimentary interbed at the depth of about 55 m is a clear indication of flow through the vadose zone. The wide range of the times (from 10 to more than 30 days) of water appearance at the depth of 55 m indicates that water flowed nonuniformly through the vadose zone. The difference in the water and tracer arrival time can be attributed to changes in the flow pathways with time.

The practical application of the large-scale investigation is to understand the flow processes and develop models in order to study the distributed flow and contaminant transport problems that exist under the RWMC and elsewhere at INEEL or in the tank farms at Hanford.

10. Conclusions

All laboratory and field infiltration tests showed that a typical feature of flow in fractured rocks is channeling that occurs at all scales of investigation, including individual fractures, the intra-basalt fracture network, and the inter-basalt rubble-zone network. However, the instrumentation used in laboratory and small-scale field conditions (in particular, to record dripping phenomena) is not practical for use at larger field scales. Field measurements of flow characteristics in fractured rocks using single probes (such as tensiometers) are uncertain, because the locations of the probes in relation to the flow paths are not precisely known, and these probes average fracture and matrix hydraulic characteristics.

An important feature of flow in the basalt vadose zone is that the hydraulic system includes both unsaturated and saturated rocks. During flooding at the surface, the saturated zones have a limited and local extent within flow channels in the fractures and vesicular zones. Single probes, which cross the saturated fractures, also intersect the matrix, and, hence, the probes measure an averaged water pressure in the fracture-matrix system. However, it is difficult to separate the contribution of the fracture from that of the matrix (Finsterle and Faybishenko, 1997). Using available monitoring techniques under field conditions, we cannot perfect our knowledge of initial conditions; we can only measure approximate values of different parameters (pressure, moisture content, temperature, concentrations) or determine the ranges of these parameters.

Because a variety of natural conditions affect the hydraulic processes in unsaturated, fractured basalt, field and laboratory investigations in the vadose zone should be conducted on different scales: elemental, small-scale, intermediate-scale, and large-scale. We find that, at each scale of investigation, different conceptual models for flow and transport phenomena must be used to explain the observed behavior. Because different

methods of measurement are needed, we obtain data that can be used to create models describing different flow processes with no apparent scaling principles evident; instead, a hierarchy of models is needed to discriminate between the observed flow phenomena at each of the different scales.

Fluid flow in fractured basalt of the vadose zone can be considered a nonlinear dynamic process, in which the behavior, both temporally and spatially, may be chaotic (Sposito and Weeks, 1997; Weeks and Sposito, 1997). The chaotic nature of flow results from nonlinear processes and the strong spatial and temporal variations in moisture content, hydraulic conductivity, and fracture connectedness. As a result, in fractured basalt (that is a nonlinear system) small variations in flow parameters may lead to significant variations in predicted results. The dissipative nature of the system implies that its phase-space volume decreases with time, leading to the formation of strange attractors characterizing the range in which the flow parameters are expected to change. The dynamics of such systems are sensitive to the initial conditions. The response of such systems may include a stochastic component that it is not necessarily a dominant factor on the system behavior. If the stochastic component is not dominant, then a stochastic analysis will not provide useful information.

We also find that under field conditions with a limited number of single-probe measurements, we can detect neither the spatial nor temporal chaotic variations of the flow parameters, and therefore, we must use conventional (i.e., nonchaotic) stochastic or deterministic methods to describe flow and transport processes. If the stochastic component is not a dominant factor, then a stochastic analysis will provide incorrect answers and should be replaced by a chaotic analysis. If the stochastic component is significant (or if the phase-space dimension is so large that the dynamics look stochastic), then a stochastic analysis is the most appropriate tool to use. Because the system exhibits sensitivity to initial conditions, we can predict only the range in which the flow rate is expected to change, but not the exact flow rates. Where elemental and small-scale components are involved, the flow data can be analyzed using methods of nonlinear dynamics. Where intermediate and large-scale components are involved, a combination of deterministic and stochastic methods of flow analysis can be used.

References:

Abarbanel, H.D.I., *Analysis of Observed Chaotic Data*, Springer-Verlag New York, Inc., 1996

Barenblatt, G.E., I.P. Zheltov and I.N. Kochina, Basic concepts in the theory of seepage of homogeneous liquids in fissured rocks, *Jour. Appl. Math.*, 24 (5), 1286-1303, 1960.

Barton, C.C. and E. Larsen, Fractal geometry of two-dimensional fracture networks at Yucca Mountain, southwestern Nevada, *Proc. of the International Symposium on Fundamentals of Rock Joints*, Bjorkliden, Sweden, pp. 77-84, 1985.

Bear, J., C.F. Tsang, and G. de Marsily, eds., *Flow and Contaminant Transport in Fractured Rock, Academic Press*, San Diego, CA, 1993

Birkholzer, J. and C.F. Tsang, Solute canneling in unsaturated heterogeneous porous media, *Water Resour. Res.*, *33*(10), 2221 - 2238, 1997.

Bishop, C.W. and I. Porro, Comparison of neutron moisture gauges and a neutron tool for use in monitoring wells, *Ground Water*, *35*(3), 394-400, 1996.

Bruno, B.C., G.J. Taylor, S.K. Rowland, P.G. Lucey, and S. Self, Lava flows are fractals, *Geophysics Research Letters*, *19*(3), 305-308, 1992.

Chesnut, D.A., Dispersivity in heterogeneous permeable media, *in Proceedings of the Fifth Annual International High-Level Radioactive Waste Management Conference, Las Vegas, NV*, American Nuclear Society, La Grange Park, IL, *4*, 1822-1841, 1994.

Cox, B.L. and J.S.Y. Wang, Fractal analysis of anisotropic fracture surfaces, *Fractals*, *1*(13), 547-559, 1993.

Dagan, G., *Flow and transport in porous formations*, Berlin ; New York : Springer-Verlag, 1989.

Department of Energy, Environmental Assessment, Reference Repository Location, Hanford Site, Washington, *DOE/RW-0070*, Washington, D.C., 1986.

Dershowitz, W.S., K.Redus, P. Wallmann, P. La Pointe, and C.-L.Axelsson, The application of fractal dimension in hydrology and rock mechanics, *Swedish Nuclear Fuel and Waste Management Co., Tech. Report 92-17*, Stockholm, Sweden, 1992.

Doughty, C., Ponded infiltration test in fractured basalt at the Box Canyon site: (3) Numerical modeling, *Lawrence Berkeley National Laboratory Report LBNL-40630*, 1998.

Engelder, T., Joints and shear fractures in rock, in *Fracture Mechanics of Rock*, edited by B.K. Atkinson, pp. 27-69, Academic Press, Orlando, FL, 1987.

Faybishenko, B., C. Doughty, J. Geller, S. Borglin, B. Cox, J. Peterson Jr., M. Steiger, K. Williams, T. Wood, R. Podgorney, T. Stoops, S. Wheatcraft, M. Dragila, and J. Long, A chaotic-dynamical conceptual model to describe fluid flow and contaminant transport in a fractured vadose zone, *Lawrence Berkeley National Laboratory Report LBNL-41223*, 1998.

Faybishenko, B., Hydraulic behavior of quasi-saturated soils in the presence of entrapped air: laboratory experiments, *Water Resour. Res.*, 31(10), 2421-2435, 1995.

Faybishenko, B., Evidence of chaotic behavior in flow through fractured rocks, and how we might use chaos theory in fractured rock hydrogeology, *Proceedings of the International Symposium "Dynamics of Fluids in Fractured Rocks: Concepts and Recent Advances,"* Lawrence Berkeley National Laboratory, Berkeley, CA, pp. 207-212, 1999.

Faybishenko, B., Theory and numerical evaluation of the parameters of the chaotic behavior of flow in unsaturated soils and rocks, *Abstract presented at the Chapman Conference on Fractal Scaling, Nonlinear Dynamics, and Chaos in Hydrologic Systems*, Clemson University, Clemson, SC, 1998a.

Faybishenko, B.A., R. Salve, P. Zawislanski, K.H. Lee, P. Cook, B. Freifeld, K. Williams, C. Doughty, Ponded infiltration test at the Box Canyon site: data report and preliminary analysis, *Lawrence Berkeley National Laboratory Report LBNL-40183*, 1998b.

B. Faybishenko, C. Doughty, M. Steiger, J.C.S. Long, T. Wood, J. Jacobsen, J. Lore, and P. Zawislanski, Conceptual model of the geometry and physics of water flow in a fractured basalt vadose zone: Box Canyon Site, Idaho, Paper submitted to *Water Resour. Res.*, 1999.

Faybishenko, B.A., Hydraulic behavior of quasi-saturated soils in the presence of entrapped air: laboratory experiments, *Water Resour. Res.*, *31*(10), 2421-2435, 1995.

Fedder, J., and T. Jossang, Fractal patterns in porous media, In: C.C. Barton, and P.R. La Pointe (Eds), *Fractals in Petroleum Geology and Earth Processes*, Plenum Press, New York, pp. 179-226, 1995.

Finsterle, S.and B. Faybishenko, What does a tensiometer measure in fractured rocks? *In Characterization and Measurement of the Hydraulics Properties of Unsaturated Media,* Proceedings of the International Symposium 1997, Riverside, CA, 1998.

Geller, J.T., G. Su, and K. Pruess, Preliminary studies of water seepage through rough-walled fractures, *Lawrence Berkeley National Laboratory Report LBNL-38810*, 1996.

Glass, R.J., T.S. Steenhuis, and J.Y. Parlange, Immiscible displacement in porous media: Stability analysis of three-dimensional, axisymmetric disturbances with application to gravity-driven wetting front instability, *Water Resour. Res., 27*(8), 1947-1956, 1991.

Gleick, J., *Chaos: Making a New Science*, New York, N.Y., U.S.A. : Viking, 1987.

Grassberger, P. and I. Procaccia, Characterization of strange attractors, *Phys. Rev. Letters, 50*, 346-349, 1983.

Haken, H., *Advanced Synergetics: Instability Hierarchies of Self-Organizing Systems and Devices*, Springer-Verlag, Berlin, 1983.

Hardy,H.H., and R.A. Beier, *Fractals in reservoir engineering*, World Scientific, Singapore; New Jersey, 1994.

Ho, C. K., Models of fracture-matrix interactions during multiphase heat and mass flow in unsaturated fractured porous media, *Sixth Symposium on Multiphase Transport in Porous Media, 1997 ASME International Mechanical Engineering Congress and Exposition*, Dallas, TX, 1997.

Horton, R.E., An approach toward a physical interpretation of infiltration-capacity, *Soil Sci. Soc. Am. Proc., 5*, 399-417, 1940.

Hubbard, S.S., J.E. Peterson, E.L. Majer, P.T. Zawislanski, K.H. Williams, J. Roberts, and F, Wobber, Estimation of permeable pathways and water content using tomographic radar data, *The Leading Edge of Exploration*, 16(11), 1623-1628, 1997.

Jury, W.A. and K. Roth, 1990, *Transfer Functions and Solute Movement through Soil: Theory and Applications*, Birkhäuser Verlag, Basel, Switzerland.

Kennel, M.B., R. Brown, and H.D.I. Abarabanel, Determining embedding dimension for phase-space reconstruction using a geometrical construction, *Physical Review* A, Vol. 45(6), 3405-3411, 1992.

Kilbury, R.K., T.C. Rasmussen, D.D. Evans, and A.W. Warrick, Water and air intake of surface-exposed rock fractures in situ, *Water Resour. Res.*, 22(10), 1431-1443, 1986.

Knutson, C.F., D.O. Cox, K.J. Dooley, and J.B. Sisson, Characterization of low-permeability media using outcrop measurements, in 68th Annual Technical Conference and Exhibition of the Society of Petroleum Engineers, October 3-6, 1993, Houston, TX, *SPE Paper 26487*, 1993.

Korvin, G., *Fractal Models in the Earth Sciences*, Elsevier, Amsterdam, 1992.

Kwicklis, E. and R.W. Healey, Numerical investigation of steady liquid water flow in a variably saturated fracture network, *Water Resour. Res., 29*(12), 4091-4102, 1993.

Lenormand, R. and C. Zarcone, Capillary fingering: percolation and fractal dimension, *Transport in Porous Media, 4*, 599-612, 1989.

Long, J.C.S., C. Doughty, B. Faybishenko, A. Aydin, B. Freifeld, K. Grossenbacher, P. Holland, J. Horsman, J. Jacobsen, T. Johnson, K. -H. Lee, J. Lore, K. Nihei, J. Peterson, Jr., R. Salve, J. Sisson, B. Thapa, D. Vasco, K. Williams, T. Wood, and P. Zawislanski, Analog site for fractured rock characterization, Annual Report FY 1995, *Lawrence Berkeley National Laboratory Report LBNL-38095*, 1995.

Long, J.C.S., J. Remer, C. Wilson, and P.A. Witherspoon, Porous media equivalents for networks of discontinuous fractures, *Water Resour. Res., 18*(3), 645, 1982.

Long, P. and B. Wood, Structures, textures, and cooling histories of Columbia River basalt flows. *Geological Society of America Bulletin, 97*, 1144-1155, 1986.

Majer, E.L., J.E. Peterson, T. Daley, B. Kaelin, L. Myer, J. Queen, P. D'Onfro, and W. Rizer, Fracture detection using crosswell and single well surveys, *Geophysics, 62* (2), 495-504, 1997.

Mantoglou, A. and L.W. Gelhar, Capillary tension head variance, mean soil moisture content, and effective specific soil moisture capacity of transient unsaturated flow in stratified soils, *Water Resour. Res., 23*(1), 47 - 56, 1987a.

Mantoglou, A. and L.W. Gelhar, Effective hydraulic conductivities of transient unsaturated flow in stratified soils, *Water Resour. Res., 23*(1), 57 - 67, 1987b.

Molz, F.J., and G.K. Boman, Further evidence of fractal structure in hydraulic conductivity distributions, *Water Resour. Res., 22*(18), 2545-2548, 1995

Moon, F.C., *Chaotic Vibrations, an Introduction for Applied Scientists and Engineers*, John Wiley, New York, 1987.

National Research Council, *Rock Fractures and Fluid Flow*, Edited by J. Long et al., National Academy Press, Washington, DC, 1996.

Nativ, R., E. Adar, O. Dahan and M. Geyh, Water recharge and solute transport through the vadose zone of fractured chalk under desert conditions, *Water Resour. Res., 31*(2), 253-261, 1995.

Neuman, S.P., Generalized scaling of permeabilities: Validation and effect of support scale, *Geophysical Research Letters, 21*(5), 349-352, 1994.

Neuman, S.P., Universal scaling of hydraulic conductivities and dispersivities in geologic media, *Water Resour. Res., 26(8),* 1749-1758, 1990.

Newman M.E. and F.M. Dunnivant, Results from the large-scale aquifer pumping and infiltration test: transport of tracers through fractured media, *Idaho National Engineering Laboratory Report INEL-95/146, ER-WAG7-77*, 1995.

Nicholl, M.J., R.J. Glass, and H.A. Nguyen, Wetting front instability in an initially wet unsaturated fracture, in *Proceedings of the Fourth High Level Radioactive Waste Management International Conference*, Las Vegas, NV, 1993.

Nicholl, M.J., R.J. Glass, and S.W. Wheatcraft, Gravity-driven infiltration instability in initially dry nonhorizontal fractures, *Water Resour. Res.*, 30(9), 2533-2546, 1994.

Nolte, D.D., L.J. Pyrak-Nolte, and N.W.G. Cook, The fractal geometry of flow paths in natural fractures in rock and the approach to percolation, *Pure and Applied Geophysics, 131*, (1/2), 111-138, 1989.

Pasternak, G.B., Assessing claims for chaos in hydrologic records, *Hydrology Days*, 395-406, 1996.

Persoff, P. and K. Pruess, Two-phase flow visualization and relative permeability measurement in natural rough-walled rock fractures, *Water Resour. Res., 31*(5), 1175-1186, 1995.

Peters, R.R. and E.A. Klavetter, A continuum model for water movement in an unsaturated fractured rock mass, *Water Resour. Res., 24*(3), 416-430, 1988.

Peterson, J.E. and K.H. Williams, Ground penetrating radar results at the Box Canyon site: 1996 survey as part of infiltration test, *Lawrence Berkeley National Laboratory Report LBNL-40915*, 1997.

Podgorney, R., and T.R. Wood, Observations of Water Movement in Variably Saturated Fractured Basalt and Its Possible Implications on Predictive Modeling, *Proceedings of the International Symposium "Dynamics of Fluids in Fractured Rocks: Concepts and Recent Advances,"* Lawrence Berkeley National Laboratory, Berkeley, CA, pp. 300-304, 1999.

Podgorney, R., T.R. Wood, and T.Stoops, *1997 Outcrop infiltration experiments*, Data Summary Report, 1997.

Priest, S.D., *Discontinuity Analysis for Rock Engineering*, Chapman and Hall, London, 1993.

Pruess, K. and T. N. Narasimhan. A practical method for modeling fluid and heat flow in fractured porous media, *Society of Petroleum Engineers Journal, 25* (1), 14-26, 1985.

Pruess, K. and Y.W. Tsang, On two-phase relative permeability and capillary pressure of rough-walled rock fractures, *Water Resour. Res.*, 26(9), 1915-1926, 1990.

Pruess, K., *TOUGH User's Guide*, Nuclear Regulatory Commission Report NUREG/CR-4645; also *Lawrence Berkeley Laboratory Report No. LBL-20700*, 1987.

Pruess, K., TOUGH2 - A general purpose numerical simulator for multiphase fluid and heat flow, *Lawrence Berkeley Laboratory Report LBL-29400*, Lawrence Berkeley Laboratory, Berkeley, CA, 1991.

Pruess, K., On water seepage and fast preferential flow in heterogeneous, unsaturated rock fractures, *Jour. of Contam. Hydr.*, 30, 333-362, 1998.

Pruess, K., B. Faybishenko, and G.S. Bodvarsson, Alternative concepts and approaches for modeling flow and transport in thick unsaturated zones of fractured rocks, *Jour. of Contam. Hydrology*, May 1999.

Pruess, K., J.S.Y. Wang and Y.W. Tsang, Effective Continuum aproximation for modeling fluid and heat flow in fractured porous tuff, *Report No. SAND86-7000*, Sandia National Laboratories, Albuquerque, NM, 1988.

Pyrak-Nolte, L.J. D.D.Nolte, and N.G.W.Cook, Hierarchical cascades and the single fracture: Percolation and seismic detection, I*n: C.C.Barton, and P.R. La Pointe (Eds), Fractals in Petroleum Geology and Earth Processes*, Plenum Press, New York, pp. 143-178, 1995.

Rasmussen, T., Computer simulation model of steady fluid flow and solute transport through three-dimensional networks of variably saturated, discrete fractures, *in Flow and*

Transport through Unsaturated Fracture Rock, D. Evans and T. Nicholson, eds., American Geophysical Union, Geophysical Monograph 42, pp. 107-114, 1987.

Sahimi, M., Flow, dispersion, and displacement processes in porous media and fractured rocks: From continuum models to fractals, percolation, cellular automata and simulated annealing, *Reviews of Modern Physics, 65* (4), 1393-1534, 1993.

Shaw, R., *The Dripping Faucet as a Model Chaotic System*, Aerial Press, Santa Cruz, CA, 1984.

Smith, L. and F. Schwartz, Solute Transport through Fracture Networks, in: *Flow and Contaminant Transport in Fractured Rock*, Academic Press, 1993.

Sposito, G., and S.W. Weeks, Dynamical systems theory and fluid flow in subsurface zones, *Proceeding of 1997 Fall American Geological Union Meeting* , San Francisco, F247, 1997.

Su, G., J.T. Geller, K. Pruess, and F. Wen, Experimental studies of water seepage and intermittent flow in unsaturated, rough-walled fractures, submitted to *Water Resour. Res.*, 1998.

Tomkeieff, S.I., The basalt lavas of the Giant's Causeway district of Northern Ireland, *Bulletin Volcanolojique, 2*(6), 89-146, 1940.

Tokunaga, T. K. , and J. Wan, Water film flow along fracture surfaces of porous rock *Water Resour. Res.*, Vol. 33(6), p. 1287-1295, 1996.

Tsonis, A.A., *Chaos: From Theory to Applications, Plenum Press*, 1992.

Wang, J.S.Y. and T.N. Narasimhan, Unsaturated flow in fractured porous media, in: *Flow and Contaminant Transport in Fractured Rock*, Academic Press, 1993.

Warren, J.E., P. J. Root, The behavior of naturally fractured reservoirs, *Soc. Pet. Eng. J., Transactions, AIME, 228*, 245-255, 1963.

Weeks, S.W., and G.Sposito, Mixing and stretching efficiency in steady and unsteady subsurface fluid flows, *Proceeding of 1997 Fall American Geological Union Meeting* , San Francisco, F247, 1997.

Welhan, J.A., and M.F. Reed, Geostatistical analysis of regional hydraulic conductivity variations in the Snake River Plain aquifer, eastern Idaho, *GSA Buletin, 109,* (7), 855-868, 1997.

Witherspoon, P.A., J.S.W. Wang, K. Iwai, and J.E. Gale, Validity of cubic law for fluid flow in a deformable rock fracture, *Water Resour. Res., 16*(6), 10106-1024, 1980.

Wood, T.R., and G.T.Norrell, Integrated large-acale aquifer pumping and infiltration tests, *Groundwater Pathways OU 7-06. Summary Report, INEEL-96/0256*, Lockheed Martin Idaho Technologies Company, Idaho, 1996.

Yeh, T.C.J., L.W. Gelhar, and A.L. Gutjahr, Stochastic analysis of unsaturated flow in heterogeneous soils, 3, Observations and applications, *Water Resour. Res., 21*(4), 465 - 471, 1985.

10. Acknowledgments

The authors would like to thank Michael Steiger for participation in the Box Canyon infiltration test, Sharon Borglin for conducting laboratory experiments, Janet Jacobsen and Lea Cox for their help in interpretation of the LSIT data, and Karsten Pruess and Stefan Finsterle of LBNL and Tom Stoops of INEEL for many useful discussions.

Reviews and suggestions for improvement by Karsten Pruess and Curt Oldenburg are very much appreciated. This work was funded by the Office of Environmental Management, Office of Science and Technology, Characterization, Monitoring, and Sensor Technology Crosscutting Program, and the Environmental Management Science Program of the U.S Department of Energy under Contract No. DE-AC03-76SF00098.

Captions:

Figure 1. Schematic illustration of water flow and contaminant transport in fractured basalt, including flow through inter-basalt rubble zones between basalt flows and through an intra-basalt flow fractures pattern. Note that perched water zones are formed above the sedimentary layer.

Figure 2. Geological features and processes of water flow and chemical transport in fractured basalt: 1-flow through near-surface soil-infilled fractures, 2-fracture-to-matrix diffusion, 3-flow in a horizontal fracture connecting vertical fractures, 4-vesicular basalt-to-massive basalt diffusion, 5-funneling effect, 6-vesicular basalt-to-nonconductive fracture diffusion, 7-conductive fracture-to-vesicular basalt flow and diffusion, 8-lateral flow and advective transport in the central fracture zone, 9-lateral flow and advective transport in the rubble zone, and 10-flow in the underlying basalt flow.

Figure 3. A four-level hierarchy of scales of hydrogeological components in fractured basalt.

Figure 4. Time-series functions (left) and their two-dimensional attractors (right): (a) sine function, (b) sine function with noise, (c) random function, and (b) chaotic system from a set of Lorenz equations.

Figure 5. Video images of a cycle of water dripping within a flow channel along a dense basalt fracture surface mated to a transparent replica of the second half of the fracture. Time is given in the left-bottom corner of each image. Water was applied at 0.33 mL/hr to the top of the fracture. Fluorescein was added to the water to promote visualization by near-UV light. The fracture was inclined at 20^{o} from the horizontal.

Figure 6. Experimental setup for monitoring water-dripping in fracture models: (a) The fracture model is 20 cm x 30 cm glass plate pairs, smooth or textured, separated by 0.35 mm shims; the model is inclined 60^{o} from the horizontal; (b) Time-series of water pressure measured at the entrance to the capillary tube and corresponding video images of drip formation. Note that the water thread snaps when the pressure is minimal. We assume that the weight of the water drop overcomes capillary forces arising from the presence of the small fracture model aperture.

Figure 7. Time-series data (above) and attractors (below) for 0.25 mL/hr flow rate through 0.18 mm ID capillary tube: (a) Open-air drips, (b) Constant aperture, 0.35 mm,

glass plate pair, and (c) Variable aperture, 0-1 mm, fracture model. As the geometry surrounding the tube becomes more complex, the magnitude of pressure fluctuations increases and the attractors change from noisy to more deterministic chaotic.

Figure 8. Design of a small-scale infiltration test at the Hell's Acre site in Idaho and the types of measurements conducted: 1-Water level and infiltration rate in the water gallery, 2-Basalt-matrix water pressure using tensiometers, 3-Fracture-matrix water pressure using tensiometers, 4-Temperature of rocks, 5-Ambient air and water temperature, 6-Barometric pressure, 7-Precipitation, 8-Outflow drip intervals, and 9-Outflow volumetric flow rate in 20x30 cm pans.

Figure 9. Results of a small-scale infiltration test: (a) Infiltration rate, (b) Outflow rates in several pans, and (c) Tensiometer pressure.

Figure 10. Variations of time-intervals of water dripping: (a) time-series data (only first 300 points are shown), (b) a 2D attractor using $\tau = 3$, which was plotted using 2,000 points.

Figure 11. Fracture map of the basalt flow outcrop at the Box Canyon site located about 30 m from the research site, and a photograph of the infiltration pond. Figure shows that the width of the infiltration pond was about twice as much as the width of the largest basalt columns.

Figure 12. A conceptual model of the fracture pattern showing the vertical and horizontal fractures and fracture zones, as well as dead-end fractures. The locations of dead-end fractures are arbitrary.

Figure 13. An example of the radar velocities between two boreholes located four meters apart just outside the pond. The red color indicates low radar velocity zones associated with a higher moisture content, and the blue color indicates higher velocity zones with a lower moisture content. The field data were taken in October 1998 by K.H. Williams, and the data inversion was conducted by J. Peterson of LBNL.

Figure 14. Schematic presentation of types of measurements in fractured rocks using: 1-Point-type, passive, probes (tensiometers, ER and TDR) of a 5-20 cm size, which detect water only if water contacts the probe; 2-Near-borehole moisture content measurements using neutron logging, and water sampling using suction lysimeters within the distance of 30-40 cm from the borehole; and 3-Cross-borehole radar and 3D ER tomography on the distance up to 10-12 m.

Figure 15. The geometry and types of rocks (a) used for the 2-D modeling of Box Canyon infiltration test, and breakthrough curves (b) obtained for different locations. Location numbers on figure (a) correspond to numbers of breakthrough curves on figure (b).

Figure 16. General layout of the infiltration pond and the borehole monitoring system during the LSIT, and breakthrough curves of Se-75 determined in boreholes screened in a perched water zone.

Figure 17. The relationship between the time of water arrival (determined from neutron logging) and the Se-75 tracer arrival (determined from water sampling) and depth.

Figure 18. A conceptual model (a) of the fracture pattern and corresponding breakthrough curves (b) for Se-75 for several locations shown on the conceptual model in figure (a).

Figure 19. A conceptual model of a field infiltration test showing water dripping, which can be considered as an elemental component, and a collection of water into pans that can be considered as a small-scale component.

ERNEST ORLANDO LAWRENCE BERKELEY NATIONAL LABORATORY
ONE CYCLOTRON ROAD · BERKELEY, CALIFORNIA 94720

Prepared for the U.S. Department of Energy under Contract No. DE-AC03-76SF00098